

1 **Impacts of Sea Ice Leads on Sea Salt Aerosols and Atmospheric Chemistry in the Arctic**

2 Erin J. Emme^{1,*}; Hannah M. Horowitz^{1,2,*}

3

4 ¹Department of Civil and Environmental Engineering, University of Illinois Urbana-
5 Champaign, Urbana, Illinois, USA

6 ²Department of Atmospheric Science, University of Illinois Urbana-Champaign, Urbana,
7 Illinois, USA

8

9

10

For submission to

11

Atmospheric Chemistry and Physics

12

February 6, 2025~~October 9, 2024~~

13

14

15

*Corresponding authors: Erin J. Emme, emme2@illinois.edu, and Hannah M. Horowitz,

16

hmhorow@illinois.edu.

17

18

19 **Impacts of Sea Ice Leads on Sea Salt Aerosols and Atmospheric Chemistry in the Arctic**

20 **Erin J. Emme¹, Hannah M. Horowitz^{1,2}**

21 **¹Department of Civil and Environmental Engineering, University of Illinois at Urbana-
22 Champaign, Urbana, 61801, USA**

23 **²Department of Atmospheric Sciences, University of Illinois at Urbana-Champaign, Urbana,
24 61801, USA**

25 **Correspondence to: Erin J. Emme (emme@illinois.edu) and Hannah Horowitz
26 (hmhorow@illinois.edu)**

27

28 **Abstract.** The processes contributing to Arctic cold season (November-April) sea salt aerosols
29 (SSA) remain uncertain. Observations from coastal Alaska suggest emissions from open leads in
30 sea ice, which are not included in climate models, may play a dominant role. Their Arctic-wide
31 significance has not yet been quantified. Here, we create an emissions parameterization of SSA
32 from leads by combining satellite data of lead area (the AMSR-E product) and a chemical
33 transport model (GEOS-Chem) to quantify pan-Arctic SSA emissions from leads during the cold
34 season from 2002-2008 and predict their impacts on atmospheric chemistry, evaluating the
35 results of our simulated SSA against in-situ observations. The AMSR-E product detects large
36 leads with certainty (>3 km in size) and hence our study is limited to quantifying emissions from
37 large leads. Lead emissions vary seasonally and interannually. Simulated total monthly SSA
38 emissions increase by 1.1-1.8% ($\geq 60^\circ\text{N}$ latitude) and 5.6-7.5% ($\geq 75^\circ\text{N}$) for the 2002-2008 cold
39 season. SSA concentrations increase primarily at the location of leads, where standard model
40 concentrations are low. GEOS-Chem overestimates SSA concentrations at Arctic sites compared
41 to ground observations even when lead emissions are not included, suggesting underestimation
42 of SSA sinks and/or uncertainties in SSA emissions from blowing snow and open ocean. Multi-
43 year monthly mean surface bromine atom (Br) concentrations increase 2.8-8.8% due to SSA
44 from leads for the 2002-2008 cold season. Changes in ozone concentrations are negligible. While
45 leads contribute <10% to Arctic-wide SSA emissions in the years 2002-2008, these emissions
46 occur in regions of low background aerosol concentrations. Leads may increase in frequency
47 under future climate change, which could increase SSA emissions from leads.

48

49 **Short Summary**

50 There is uncertainty in the sources of Arctic cold season (November-April) sea salt aerosols.
51 Using a chemical transport model and satellite observations, we quantify Arctic-wide sea salt
52 aerosol emissions from fractures in sea ice, called open sea ice leads, and their atmospheric

53 chemistry impacts for the cold season. We show sea ice leads contribute to Arctic sea salt
54 aerosols and bromine, especially in under-observed regions.

55

56 1. Introduction

57

58 Sea salt aerosols (SSA) affect Arctic climate by scattering incoming solar radiation and acting as
59 cloud condensation nuclei and ice nuclei (DeMott et al., 2016; Pierce and Adams, 2006; Quinn et
60 al., 1998). ~~While in the Arctic there is no sunlight during polar night to scatter radiation, cloud
61 condensation nuclei and ice nuclei can still have impacts on clouds and longwave radiation in the
62 Arctic, these processes are relevant during the fall and spring, but negligible during polar night,
63 when there is no sunlight.~~ Long-term measurements have shown that peak SSA concentrations
64 in the Arctic occur during the cold season (Leitch et al., 2018; Quinn et al., 2002; Schmale et al.,
65 2021). However, the sources and mechanisms of cold season SSA emissions are uncertain,
66 which hinders atmospheric chemistry and climate models from accurately representing polar
67 regions. Recent observations from Utqiagvik, Alaska have suggested that open leads, or open
68 sea ice fractures, are an important source of cold season SSA emissions (Kirpes et al., 2019; May
69 et al., 2016). Climate change has impacted the Arctic by rapidly decreasing sea ice age and
70 thickness (Intergovernmental Panel On Climate Change, 2023; Sumata et al., 2023; Vaughan et
71 al., 2013), and future projections indicate this will continue (Intergovernmental Panel On Climate
72 Change, 2023), suggesting the amount of open leads will increase in the future due to thinner ice
73 that is prone to fracture. More work is needed to discern the Arctic-wide importance and impacts
74 of SSA emissions from sea ice leads (“lead emissions”) on atmospheric chemistry and climate.
75 By combining satellite observations and chemical transport modeling, we quantify the significance
76 and impacts of lead emissions on atmospheric concentrations of SSA and bromine and evaluate
77 simulated SSA against in-situ observations.

78

79 While global models have not yet included SSA emissions from leads, several observational
80 studies largely based in Utqiagvik, Alaska suggest emissions of SSA from leads may be
81 important. Key early observations in the 1970s in Utqiagvik, by Scott & Levin (1972) and Radke
82 et al. (1976) demonstrated an increase in sodium-containing particles in the presence of open
83 water leads. Since then, more recent measurement studies have quantified SSA emissions from
84 leads. Nilsson et al. (2001) estimate that leads contribute an order of magnitude less than the
85 open ocean to the Arctic SSA flux during the summer months. A multi-year study of observed
86 SSA at Utqiagvik (May et al., 2016), conducted over all seasons, found that leads are a significant

Field Code Changed

Field Code Changed

Field Code Changed

Field Code Changed

Field Code Changed

87 contributor to SSA through wind-driven production, increasing the supermicron range in particular,
88 but to a lesser extent than wind-driven production from the open ocean. Willis et al. (2018) suggest
89 that lead emissions are more important in winter and early spring as winds over the Northern
90 oceans are at their highest. Kirpes et al. (2019) also convey the importance of seasonality,
91 identifying SSA produced by local leads as the dominant aerosol source in the coastal Alaskan
92 Arctic during winter months. Chen et al. (2022), focusing on the spring, ~~shows~~ at Utqiaġvik, ~~shows~~
93 ~~that~~ leads were present locally throughout the study and contributed to sea spray aerosol
94 production. As ground-based observations in the Arctic are mainly limited to coastal stations, such
95 as Utqiaġvik, it is difficult to estimate the significance and impacts of lead emissions over the
96 entire Arctic. Representing Arctic-wide emissions from leads in a global chemical transport model,
97 especially during the cold season, will help discern whether lead emissions and their impacts on
98 atmospheric chemistry are significant enough to warrant inclusion in chemistry as well as climate
99 models.

100

101 Other modeling studies in the Arctic and observations primarily from Antarctica suggest blowing
102 snow is a potential major contributor of cold season SSA in polar regions. Blowing snow SSA
103 comes from saline snow over sea ice that is swept up by wind; the snow becomes salty through
104 the upward movement of brine from sea ice to the snow surface, incorporation of frost flowers,
105 and deposition of SSA from the nearby open ocean (Domine et al., 2004). In two chemical
106 transport models, the inclusion of additional SSA emissions from blowing snow brought simulated
107 SSA mass concentrations closer to what was observed (Confer et al., 2023; Huang et al., 2018;
108 Huang and Jaeglé, 2017; Rhodes et al., 2017). Other potential sources of cold season SSA, such
109 as frost flowers, have been found to be insignificant (Alvarez-Aviles et al., 2008; Roscoe et al.,
110 2011; Yang et al., 2017). Incorporating blowing snow SSA emissions into models has shown how
111 missing sources of SSA in the Arctic can have a significant impact on atmospheric chemistry; for
112 example, Huang et al. (2020) show bromine released by blowing snow impacts modeled
113 springtime bromine activation and ozone depletion events. The strong observational evidence
114 that leads contribute to cold season SSA and the impact of blowing snow SSA on modeled Arctic
115 atmospheric chemistry suggests there is a need to assess the potential impacts of lead emissions,
116 which are currently missing from global chemistry and climate models. One study incorporated
117 SSA emissions from leads in a chemical transport model (WRF-Chem), but the study was limited
118 to the 400 km² area surrounding Utqiaġvik, Alaska and used ERA-5 reanalysis sea ice fraction to
119 define the presence of leads (Ioannidis et al., 2023). They find open leads are the primary source

Field Code Changed

120 of fresh and aged SSA in Utqiagvik, Alaska during the cold season, consistent with the
121 observational analyses by May et al. (2016) and Kirpes et al. (2019).

122

123 SSA play a critical role in Arctic tropospheric chemistry. SSA debromination is the main global
124 source of reactive bromine in the troposphere (Wang et al., 2021). Reactive bromine chemistry
125 has been attributed to the rapid depletion of ozone in the Arctic springtime, which reaches a
126 maximum in March-April (Simpson et al., 2007). In particular, bromine atom (Br) is key to these
127 ozone depletion events; it is produced through the photolysis of Br₂, which is sourced from SSA
128 debromination and snowpack chemistry (Abbatt et al., 2012; Dibb et al., 2010; Pratt et al., 2013;
129 Stutz et al., 2011). Swanson et al. (2022) show improved springtime model-observation
130 agreement of BrO by including a snowpack photochemistry mechanism based on multiple field
131 observations in a global chemical transport model. While on a global scale, reaction of OH with
132 other SSA-sourced bromine species can also produce Br (Wang et al., 2021), this is minor in polar
133 regions due to low OH concentrations. Br rapidly depletes ozone through heterogeneous
134 reactions, which produces BrO that can photolyze to reform Br, creating a catalytic ozone-
135 depletion cycle (Simpson et al., 2007).

Field Code Changed

Field Code Changed

Field Code Changed

136

137 Here, we estimate the pan-Arctic contribution of leads to total SSA emissions during the cold
138 season for the years 2002-2008, by using satellite observations of lead area to parameterize lead-
139 based SSA production in the global chemical transport model GEOS-Chem. We evaluate
140 simulated SSA concentrations against observations and predict the impacts of lead SSA
141 emissions on atmospheric chemistry, including concentrations of Br and ozone.

142

143 **2. Methods**

144

145 *2.1 Satellite Data of Lead Area Fractions*

146

147 In this study, we use satellite data of lead area fractions to inform the GEOS-Chem chemical
148 transport model (next section) of where leads are present. The Advanced Microwave Scanning
149 Radiometer-Earth Observation System (AMSR-E) sensor aboard NASA's Aqua satellite recorded
150 brightness temperatures from Earth from 2002-2011 at six different frequencies
151 (<https://www.cen.uni-hamburg.de/en/icdc/data/cryosphere/lead-area-fraction-amsre.html>)
152 (Integrated Climate Data Center (ICDC) et al., n.d.), which are converted to lead area fractions
153 following the algorithm of Röhrs and Kaleschke (2012). This method of detection can only be

154 applied to the Arctic freezing season (November-April) due to surface melt of the sea ice modifying
155 the sea ice emissivity from May-October, which affects the lead detection algorithm. Daily data is
156 available at 6.25 km horizontal resolution, as the algorithm is not limited by cloud cover. The
157 AMSR-E satellite data is regridded to 0.5°x0.625° from 6.25x6.25 km using a distance-weighted
158 average remapping for consistency with the emission model's resolution (see Sect. 2.2 below for
159 model details). For the rare individual days with missing data in the dataset (0.8%), we use the
160 average lead area fraction for that month. The lead area fraction includes open water leads and
161 thin ice-covered leads 3 km and wider. The data spans latitudes 41° to 90°N, though a majority
162 of Arctic sea ice lies above 60°N and leads are therefore unlikely to be present at lower latitudes.

163
164 We use the AMSR-E lead area product for this study as it avoids cloud interference when
165 detecting leads and provides nearly consistent daily resolution. A limited quantitative validation
166 by Röhrs and Kaleschke (2012) of one day (March 21, 2006) of the AMSR-E product against
167 Moderate Resolution Image Spectroradiometer (MODIS) showed 50% of the total lead area
168 visible in 500 m MODIS images was detected in the AMSR-E product. Leads greater than 3 km
169 in size ("large leads") were detected with certainty for the AMSR-E product (Röhrs and Kaleschke,
170 2012), so our results effectively estimate emissions from large leads only.

171

172 2.2 GEOS-Chem: global chemical transport model

173

174 Here we use the 3-D atmospheric transport model GEOS-Chem (geos-chem.org) version 13.2.1
175 (<https://doi.org/10.5281/zenodo.5500717>). Within GEOS-Chem, the Harmonized Emissions
176 Component (HEMCO) computes emissions for different sources, regions, and species (Keller et
177 al., 2014). GEOS-Chem and HEMCO are driven by Modern-Era Retrospective Analysis for
178 Research and Applications (MERRA-2) (Gelaro et al., 2017) meteorological fields from the NASA
179 Global Modeling and Assimilation Office (GMAO), which is reanalysis meteorological data
180 assimilated from various observational sources (i.e., satellite, aircraft campaigns, and ground
181 stations) providing variables such as temperature, wind, precipitation, and humidity. GEOS-Chem
182 represents one-way interactions between the MERRA-2 meteorology and chemical constituents,
183 meaning the meteorological conditions can affect the concentration of chemical species but not
184 vice versa.

185

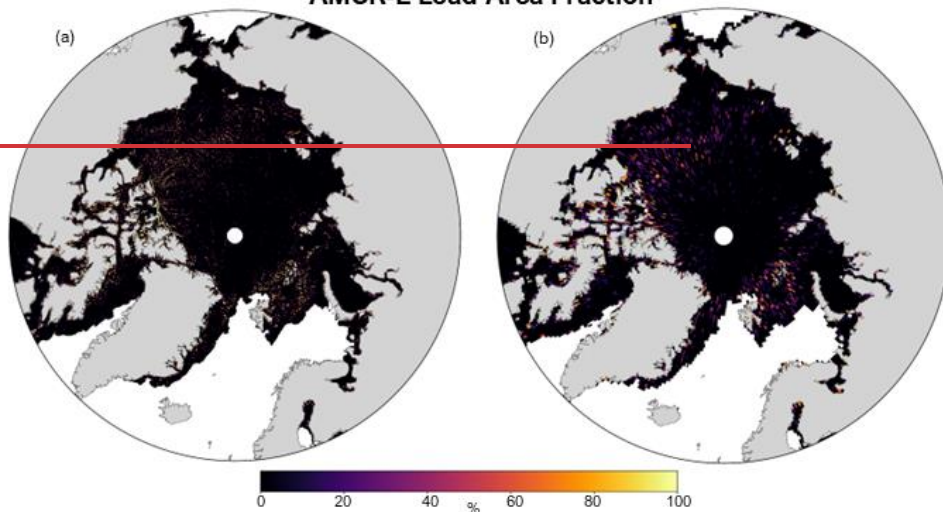
186 SSA emissions calculations for the open ocean use a wind- (Gong, 2003; Monahan et al., 1986)-
187 and sea-surface-temperature-dependent (Jaeglé et al., 2011) source function. In polar regions,

188 SSA emissions from blowing snow are also included (Huang and Jaeglé, 2017). SSA have two
189 size bins: coarse mode (SALC; $r= 0.5$ to $10 \mu\text{m}$) and accumulation mode (SALA; $r= 0.1$ to 0.5
190 μm). For gas and aerosol species, wet deposition (both rain and snow) includes washout and
191 rainout in convective and large-scale stratiform precipitation (Amos et al., 2012; Liu et al., 2001;
192 Wang et al., 2014). From November to April in the Arctic, wet deposition is mainly in the form of
193 snow (Screen and Simmonds, 2012). Dry deposition of gas and aerosol species follows a
194 resistance-in-series approach, and includes gravitational settling of sea salt (Jaeglé et al., 2011;
195 Pound et al., 2020; Wang et al., 1998; Zhang et al., 2001). Coupled gas- and multiphase-reactive
196 halogen chemistry, including sea salt debromination, acid displacement, and photolysis and
197 oxidation of gas-phase inorganic bromine and chlorine species, is described in Wang et al. (2021).
198 This version of GEOS-Chem does not include snowpack chemistry as a source of reactive
199 bromine in the standard model.

200
201 We parameterize SSA emissions from leads with the same function as the open ocean emissions
202 from Jaeglé et al. (2011) (Eq. (S-1) in the Supplemental Information (SI)), scaled by the fractional
203 area of leads in each grid cell from the AMSR-E satellite data. The Jaeglé et al. (2011) function is
204 empirically derived to best match global observations in GEOS-Chem. We assume that leads emit
205 SSA at an equal rate as a function of lead area. This lead emissions parameterization is a unique
206 wind- and SST-dependent source function for calculating lead emissions, driven by satellite
207 observations defining the presence of leads. Figure 1 shows an example of the daily temporal
208 frequency and spatial resolution of the AMSR-E satellite data (both the raw (a) and regrided (b))
209 used to drive the model.

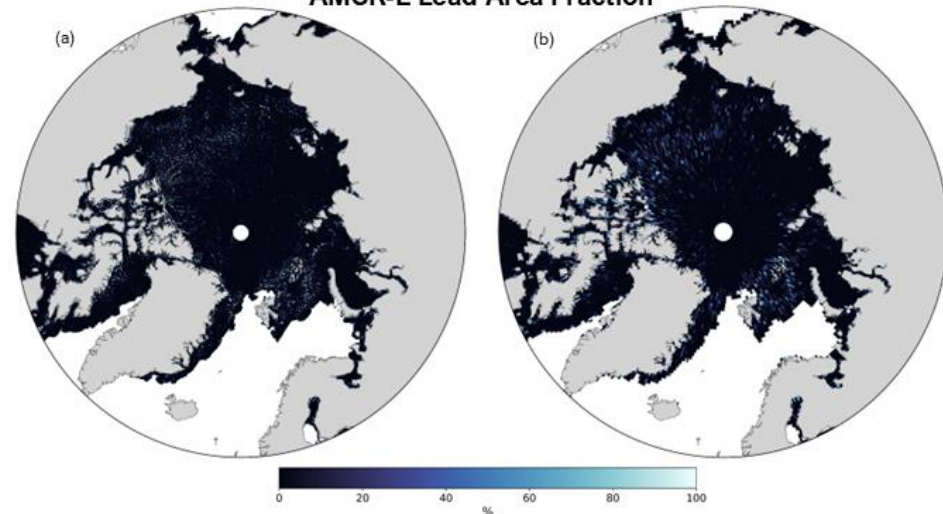
210
211

AMSR-E Lead Area Fraction



212

AMSR-E Lead Area Fraction



213

214 **Figure 1-** Map of AMSR-E daily lead area fraction in percent (%) for November 1, 2002, both raw
215 (6.25-km resolution) (a) and re-gridded (0.5°x0.625° resolution) (b).

216
217 We first calculate SSA emissions at the highest resolution of HEMCO (0.5°x0.625°), which is the
218 native resolution of MERRA-2. Two sets of emissions are calculated: (1) the standard emissions

219 only (i.e., open ocean and blowing snow SSA emissions, the “standard” case); (2) SSA emissions
220 with lead emissions added (“standard + leads” case). Each set of emissions are then implemented
221 separately into GEOS-Chem “offline” to ensure total SSA emissions are properly scaled and
222 distributed and not influenced by the resolution-dependence of the wind speed (Lin et al., 2021).
223 GEOS-Chem is run at the highest global horizontal (2° latitude x 2.5° longitude) and vertical (72
224 vertical levels) resolution. The absolute difference between the standard + leads and standard
225 simulations is the change in SSA emissions or concentration from leads, and we present the
226 percent change due to leads (%) as calculated with Eq. (1).

227

$$228 \text{ Percent change due to leads (\%)} = 100 \times \frac{(\text{Standard+leads})_{\text{simulation}} - (\text{Standard})_{\text{simulation}}}{(\text{Standard})_{\text{simulation}}} \quad (1)$$

229

230 Simulations are performed for the years 2002-2008, when there is overlap between the AMSR-E
231 satellite data and available observed Arctic SSA concentrations at multiple sites, following one
232 year of initialization. Because satellite observations of lead area fractions begin November 1,
233 2002, we initialize the standard + leads case for GEOS-Chem with standard + leads SSA
234 emissions for one year (November 1, 2002 to November 1, 2003) and then start the simulation
235 for analysis on November 1, 2002, with the spun-up November 1, 2003, initial conditions. For the
236 standard case, the initialization year begins November 1, 2001. For both cases, we simulate SSA
237 concentrations, evaluate against observed concentrations, and assess the impacts of additional
238 lead emissions on atmospheric chemistry. This includes analysis of the change in atmospheric
239 concentrations of bromine atom (Br) and ozone (O₃). For model evaluation, GEOS-Chem does
240 not track sodium (Na⁺) content for SSA, so we convert simulated SSA to Na⁺ mass concentrations
241 using a factor of $\frac{1}{3.256}$, which is based on the mass ratio of Na⁺ in seawater (Confer et al., 2023;
242 Huang and Jaeglé, 2017; Riley and Chester, 1971).

243

244 *2.3 In-Situ Observations of Arctic Sea Salt Aerosol Concentrations*

245

246 We evaluate simulated concentrations of SSA from GEOS-Chem, converted to Na⁺
247 concentrations, against in situ observations of Na⁺ concentrations at 4 Arctic sampling sites:
248 Utqiaġvik, Alaska (71.3°N, 156.6°W; 11m a.s.l.) (Quinn et al., 2002); Zeppelin Mountain, Svalbard,
249 Norway (78.9°N, 11.9°E; 475m a.s.l.) (World Meteorological Organization (WMO), 2003); Alert,
250 Nunavut, Canada (82.5°N, 62.5°W; 210m a.s.l.) (World Meteorological Organization (WMO),
251 2003); Pallas (Matorova), Helsinki, Finland (68 °N, 24.24 °E; 340m a.s.l.) (Salmi, 2018). These

Field Code Changed

252 observations are available for the time period of this study (November-April from 2002-2008,
253 except for Pallas station, 2003-2008). In winter months, the Utqiagvik, Zeppelin, and Alert coastal
254 sites border mostly ice-covered ocean (Huang and Jaeglé, 2017). At Utqiagvik, mass
255 concentrations of Na^+ for submicron and supermicron aerosols are separated, while the other two
256 sites measure the total mass concentration without size distinction. The Na^+ mass concentrations
257 are determined from ion chromatography with uncertainties of 5-11%, or an absolute uncertainty
258 of $0.01 \mu\text{g}/\text{m}^3$ (Quinn et al., 2000; World Meteorological Organization (WMO), 2003). The aerosol
259 sampling frequency is daily at Zeppelin, Utqiagvik (submicron), and Pallas and weekly at Alert
260 and Utqiagvik (supermicron).

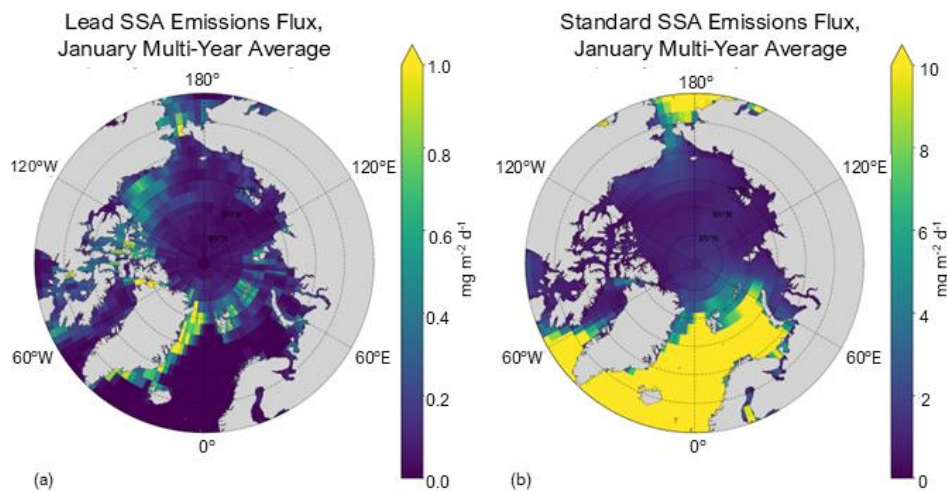
261

262 3. Results

263

264 3.1 Emissions of Sea Salt Aerosols from Leads

265



266 **Figure 2-** Total (coarse + accumulation mode) lead SSA emissions (a) and standard SSA
267 emissions (b), averaged over 2002-2008 for January. Note the difference in magnitude of the
268 colorbar of (a) and (b).
269

270

271 Figure 2a shows the spatial distribution of multi-year (2002-2008) average lead emissions for the
272 month of January, which is a climatology based on model simulations that use daily resolution

273 lead data (e.g., Fig. 1). We focus Figs. 2 and 4 on the month of January as an example. January
 274 is tied for highest lead emissions for latitudes 60°N and greater and second highest for latitudes
 275 75°N and greater (Table 1), and also has the second largest multi-year average lead area (see
 276 Fig. S-3b in SI). Alongside Fig. 2a is the standard model, which includes open ocean and blowing
 277 snow emissions (Fig. 2b; see Sect. 2.2). Total emissions are resolution independent and are
 278 shown in Fig. 2 for the 2.0°x2.5° resolution of the online atmospheric chemistry simulation. We
 279 find the lead emissions and lead area are spatially consistent (Figs. 1 and 2a) and occur in regions
 280 where the standard SSA emissions are low (e.g., in the Greenland Sea and parts of the Barents
 281 Sea). The percent change in SSA emissions due to leads (calculated with Eq. (1)) is detailed in
 282 Table 1; Figs. 4, 5, and S-4 show the percent change in SSA concentration due to leads.
 283 Generally, emissions tend to be higher from 70° to 80° N and more concentrated within the Bering
 284 Strait, Nares Strait, Wynnatt Bay in the Canadian archipelago, and the eastern Greenland Sea,
 285 as opposed to off the coast of Northern Russia and Europe. Month to month, regions where
 286 emissions are higher remains similar while the magnitude varies (see Fig. S-1 in SI).
 287

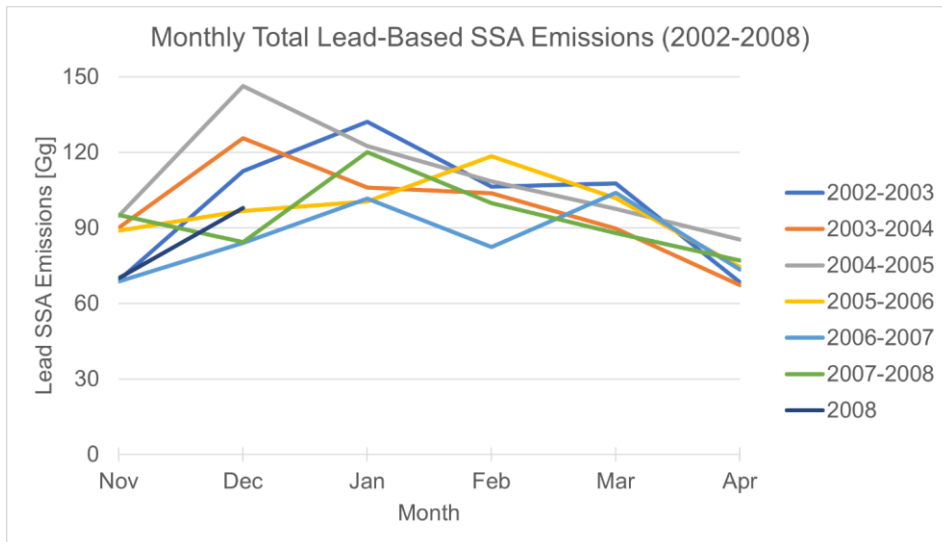
Month	Multi-Year (2002-2008) Average Standard Emissions [Gg]		Multi-Year (2002-2008) Average Lead Emissions [Gg] (and corresponding Monthly Percent Change in SSA Emissions due to Leads)	
	≥60°N	≥75°N	≥60°N	≥75°N
November	7800 ± 1000	610 ± 210	82 ± 0.14 (1.1% ± 0.14%)	42 ± 0.13 (6.9% ± 0.13%)
December	8700 ± 1400	640 ± 140	110 ± 0.20 (1.2% ± 0.20%)	48 ± 0.32 (7.5% ± 0.32%)
January	8400 ± 1100	670 ± 290	110 ± 0.10 (1.3% ± 0.10%)	46 ± 0.15 (6.9% ± 0.15%)
February	6700 ± 850	510 ± 90	100 ± 0.11 (1.5% ± 0.11%)	37 ± 0.17 (7.2% ± 0.17%)
March	6000 ± 1000	470 ± 66	98 ± 0.074 (1.6% ± 0.07%)	34 ± 0.26 (7.2% ± 0.26%)

April	4200 ± 330	400 ± 61	74 ± 0.081 (1.8% ± 0.08%)	23 ± 0.17 (5.6% ± 0.17%)
-------	------------	----------	---------------------------	--------------------------

288 **Table 1-** Multi-year (2002-2008) monthly average standard emissions and lead emissions ±1
289 standard deviation [Gg] and percent change in SSA emissions due to leads ±1 standard deviation
290 in parentheses (calculated using Eq. (1)), averaged for ≥60°N and ≥75°N.

291
292 Table 1 shows the standard and lead emissions in Gg as well as the percent change in multi-year
293 monthly average SSA emissions due to leads for 60° to 90°N latitude (≥60°N) and 75° to 90°N
294 (≥75°N). The standard deviations in Table 1 represent the year-to-year variability in emissions, as
295 the calculation is performed across the 7-year simulation time period for each month. Leads are
296 relatively more important to total SSA emissions at higher latitudes due to large open ocean
297 emissions in the North Atlantic at lower latitudes (Table 1; Fig. 2b) and the spatial variability of the
298 lead emissions (Fig. 2a). The month with the highest contribution to SSA emissions from leads
299 varies with the region being analyzed. The smaller magnitude of standard emissions later in the
300 cold season poleward of 60° N make lead emissions relatively more important, with the largest
301 percent increase ≥60° N in SSA emissions due to leads occurring in April. Poleward of 75° N, the
302 lead emissions represent a larger fraction of the standard emissions, resulting in higher percent
303 increases due to leads (~4-6% higher than for ≥60° N). Absolute lead emissions peak in December
304 for ≥75° N latitude, which is also the month with the highest percent increase due to leads ≥75°
305 N, and decrease more than twofold by April. Controlling factors of the lead emissions are
306 discussed in the next paragraph.

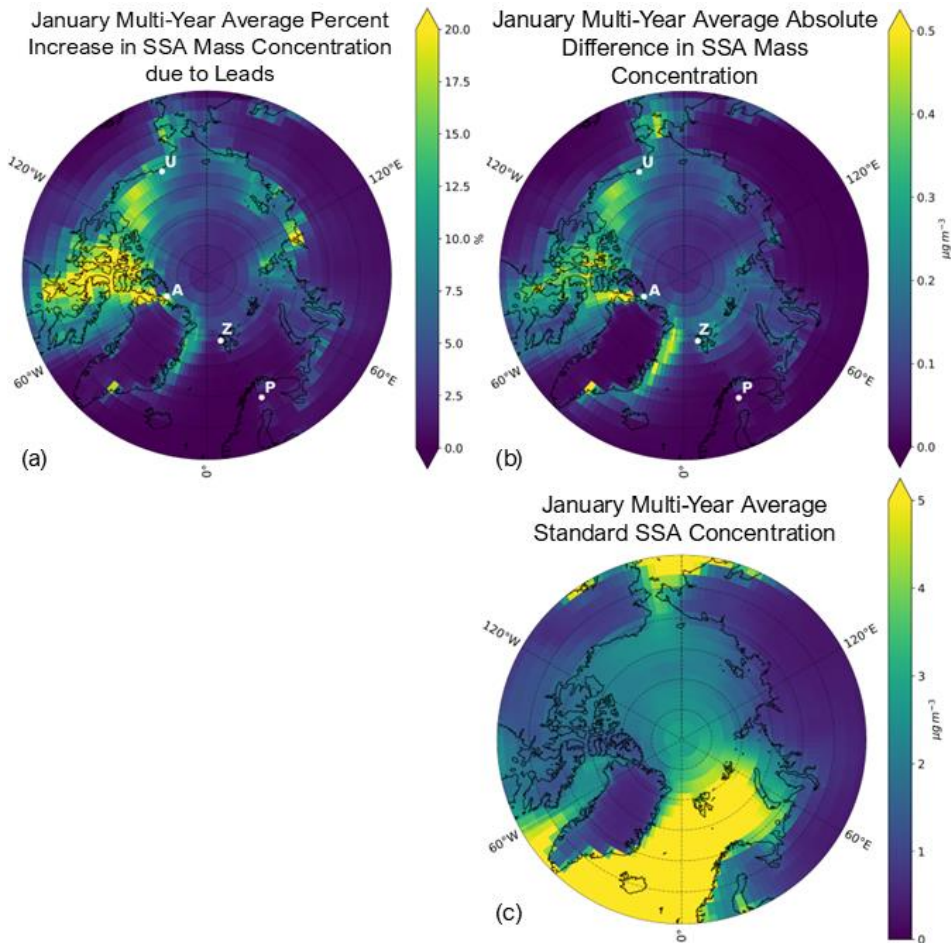
307



308
 309 **Figure 3-** Monthly variations of total (coarse + accumulation mode) lead emissions of SSA during
 310 the cold season for 2002-2008. Each line includes November and December of the first year and
 311 January through April of the following year, except for the year 2008, which only includes
 312 November and December of 2008.

313
 314 We find that the magnitude of lead emissions varies by month and year, as well as seasonally
 315 (see Fig. 3 and Figs. S-1 and S-2). Monthly total lead emissions and lead area have low correlation
 316 ($R^2= 0.13$, see Fig. S-3), indicating the variance in monthly total lead emissions is dominated by
 317 the nonlinear dependencies on wind speed and sea surface temperature (Eq. S-1 in SI), as the
 318 lead emissions are calculated with the Jaegle et al. (2011) wind speed and sea surface
 319 temperature source function. In most years, lead emissions decrease from January-April, but
 320 there is no single month when lead emissions peak each year (Fig. 3). There is also no clear
 321 interannual trend in cold season total lead emissions (see Fig. S-2). Lead emissions are lowest in
 322 the 2006-2007 cold season and highest in the 2004-2005 cold season (Fig. S-2). In the future,
 323 climate models predict that Arctic sea ice will continue to thin (high confidence) and the presence
 324 of first-year vs. multi-year sea ice will increase (very high confidence) (Intergovernmental Panel
 325 On Climate Change, 2023), suggesting a possible future increasing trend in lead area and
 326 therefore lead emissions.

327
 328 **3.2 Atmospheric Chemistry Impacts of Sea Ice Leads**



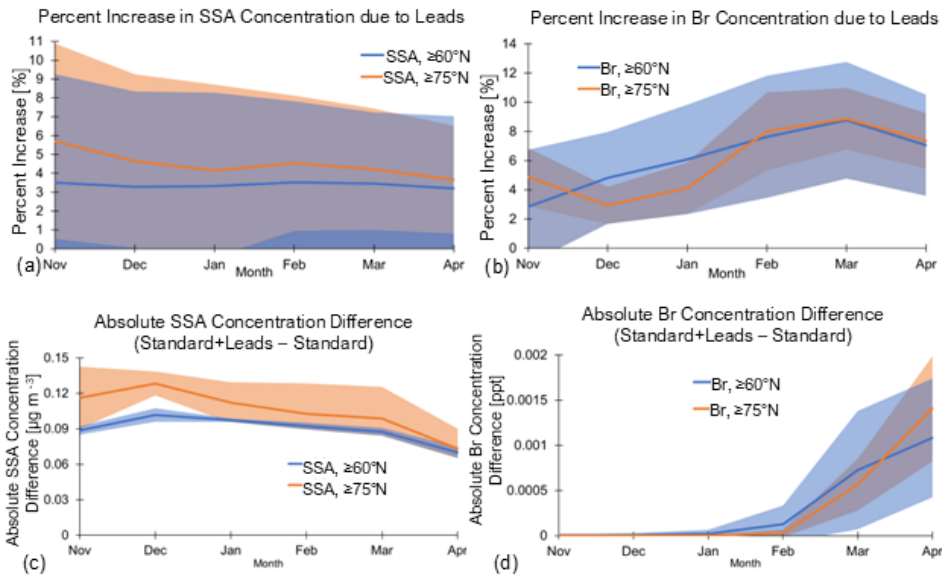
330
 331 **Figure 4-** Percent change due to leads (calculated with Eq. (1)) in SSA mass concentration (a),
 332 absolute difference between the standard+leads and standard SSA mass concentrations in $\mu\text{g m}^{-3}$
 333 (b), and the standard surface SSA mass concentration in $\mu\text{g m}^{-3}$ (c) for the January multi-year
 334 (2002-2008) average. White points in (a) and (b) represent the respective locations of each
 335 observational site: Alert, Nunavut, Canada (A); Utqiagvik, Alaska (U); Zeppelin Mountain,
 336 Svalbard, Norway (Z); Pallas (Matorova), Helsinki, Finland (P). Note the difference in magnitude
 337 of colorbars (b) and (c).
 338

339 Figure 4 shows the spatial distribution of the multi-year (2002-2008) average percent change due
340 to leads in surface SSA mass concentration (4a) and the absolute difference in SSA mass
341 concentration between the standard + leads and standard simulations (4b), as well as the
342 standard simulated SSA mass concentration (4c) for the month of January. With the addition of
343 leads, the average Arctic-wide ($\geq 60^\circ\text{N}$) percent increase in multi-year mean January SSA mass
344 concentrations is 3.3%, and the maximum percent increase in an individual model gridbox is
345 60.5%. We find that the greatest percent increases due to leads in SSA mass concentrations
346 occur at the location of lead emissions (see Fig. 2a), where the standard concentrations are also
347 very low, except off the eastern coast of Greenland, where the percent increase is reduced due
348 to the high background SSA concentrations in the Greenland Sea (Fig. 4c) from open ocean
349 emissions (Fig. 2b).

350
351 Figure 5a shows the average Arctic-wide percent increase and 5c shows the absolute difference
352 due to leads in multi-year monthly mean SSA mass concentration for each cold season month.
353 Averaged poleward of 60°N , the percent increase and absolute difference due to leads in SSA
354 mass concentration remains relatively constant throughout the cold season (Fig. 5a and c).
355 Changes in monthly mean SSA mass concentrations are also higher poleward of 75°N . However,
356 the percent increase in SSA mass concentration for both latitudinal ranges have large spatial
357 variability, as seen in the standard deviation in Fig. 5a. The spatial distribution of the percent
358 increase and absolute difference in SSA mass concentration due to leads remains similar month
359 to month (see Fig. S-4 and S-5 in SI).

360

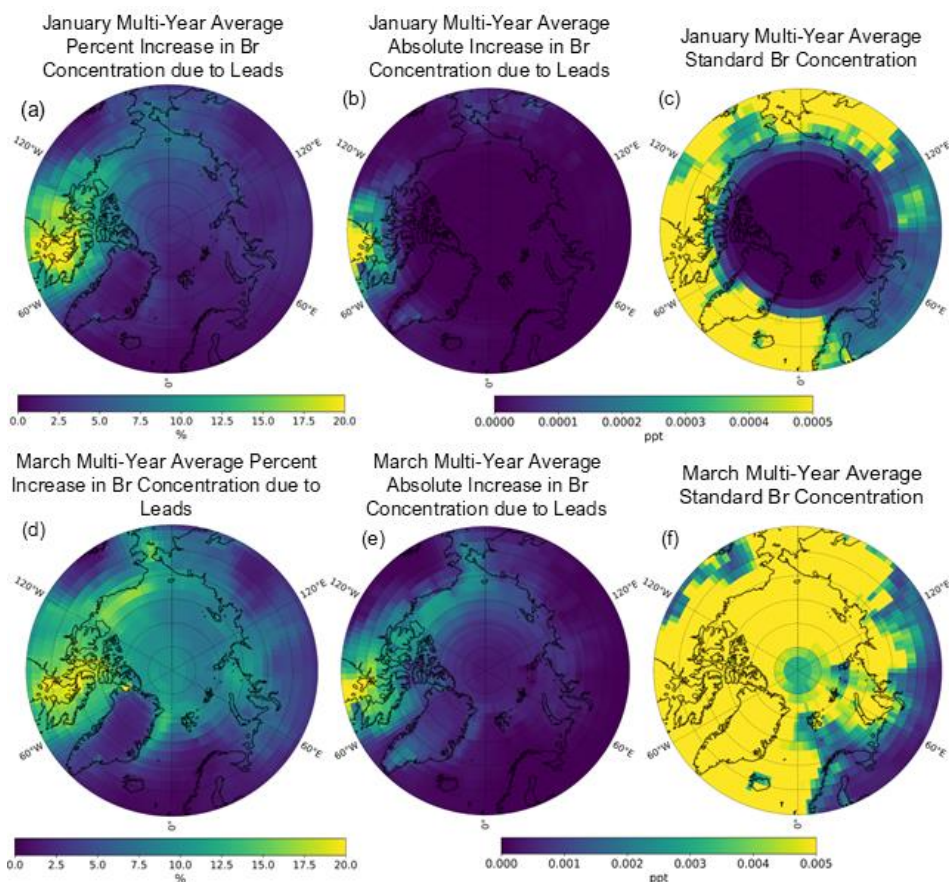
361



362
 363 **Figure 5.** Multi-year (2002-2008) monthly mean percent increase due to leads (calculated with Eq.
 364 (1)) in surface (a) SSA and (b) Br concentrations averaged across different Arctic regions (blue
 365 line: $\geq 60^\circ\text{N}$; orange line: $\geq 75^\circ\text{N}$). Shaded area represents ± 1 standard deviation.

366
 367 As described in Sect. 1, SSA contribute to the production of tropospheric reactive bromine and
 368 thereby bromine atom (Br). Here we examine changes in Br due to its role in ozone depletion
 369 events.

370



371
 372 **Figure 6-** Multi-year (2002-2008) mean January (a, b, and c) and March (d, e, and f) percent
 373 increase due to leads in surface Br concentration (a and d), absolute increase in surface Br
 374 concentration due to leads (b and e), and the standard model surface Br concentration in ppt (c
 375 and f). Note the scale of the absolute difference and standard Br concentrations for the January
 376 and March multi-year averages are an order of magnitude difference.

377
 378 Figure 6 shows the multi-year (2002-2008) mean percent increase and absolute difference due
 379 to leads in surface Br concentrations, and the standard Br concentration (in parts per trillion, or
 380 ppt) for the months of January (a-c) and March (d-f), respectively. Increased SSA from leads
 381 increases surface levels of Br across all months during the cold season (Fig. 6a, b, d, and e; Figs.
 382 S-6 and S-7 in the SI for other months). These increased concentrations spatially follow the

383 increased SSA mass concentrations from leads (Fig. 4a; Figs. S-4 and S-5 in SI for other months)
384 with differences due to where Br can be produced photochemically from the precursors released
385 from SSA. The spatial distribution of the percent increases in Br due to leads remains relatively
386 similar month to month during the cold season (see Fig. S-6 in SI), but with varying magnitude
387 (Fig. 6). The changes in Br concentration in February to April occur over a larger area (Fig. 6d
388 and e and Figs. S-6 and S-7), likely due to the seasonality of Arctic bromine chemistry, which is
389 influenced by increasing area where sunlight is available to photolyze Br-sourced SSA species.
390 The average Arctic-wide ($\geq 60^\circ\text{N}$) percent increase due to leads in multi-year January mean
391 surface Br concentration is 6.1% and the maximum increase in an individual gridbox is 35%; for
392 March, it is 8.8% and 20.4%, respectively. Overall, the average monthly percent increase in Br
393 concentration is higher than the corresponding increases in SSA concentration, particularly after
394 January, and reaches a maximum in March (see Fig. 5). The percent change due to leads in Br
395 concentrations increases from November-March poleward of 60°N and from December-March
396 poleward of 75°N (Fig. 5b). This does not strictly follow the seasonality of lead emissions (Fig. 3)
397 or the percent increase in SSA concentrations due to leads (Fig. 5a), likely due to more available
398 sunlight for photochemical reactions that produce Br later in the cold season. Increases in surface
399 Br concentration could lead to decreased surface ozone concentrations. We find that the percent
400 decrease due to leads in average surface ozone concentrations during the Arctic cold season,
401 however, are negligible ($< -0.25\%$).

402

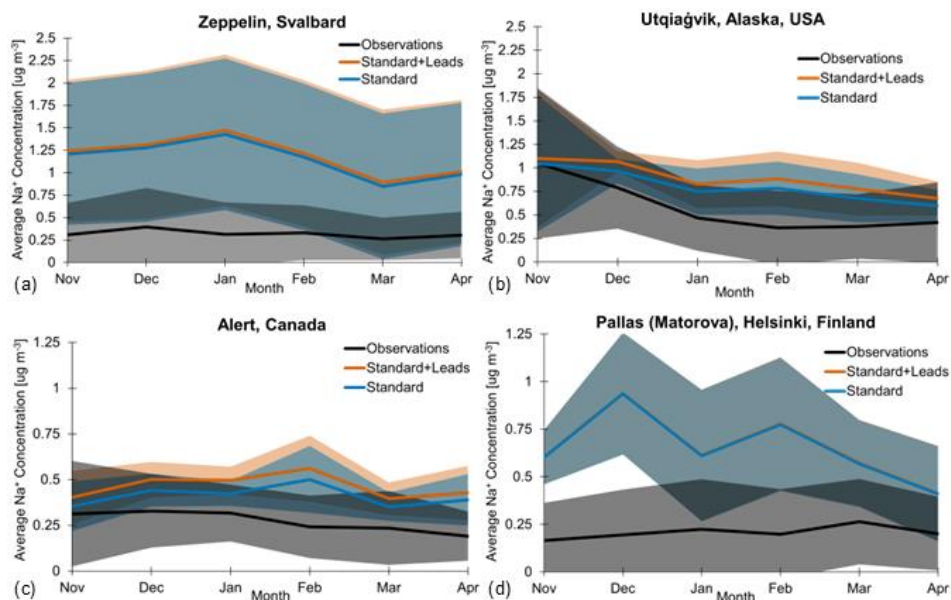
403 *3.3 Evaluation Against Sea Salt Aerosol Observations*

404

405 We compare modeled and observed sodium (Na^+) mass concentrations at four long-term
406 monitoring stations to evaluate the performance of the simulation with and without additional lead
407 emissions. The locations of each observational site are shown in Fig. 4a.

408

409



410
 411 **Figure 7-** Observed (blackline) and simulated (blue and orange lines) multi-year monthly mean
 412 sodium mass concentrations at (a) Zeppelin, Norway, (b) Utqiagvik, Alaska, (c) Alert, Canada,
 413 and (d) Pallas (Matorova), Helsinki, Finland for the cold seasons of 2002-2008 for (a)-(c) and
 414 2003-2008 for (d). Shaded regions are ± 1 standard deviation. Note the y-axis for Alert (c) and
 415 Pallas (d) are half as large as Zeppelin (a) and Utqiagvik (b).

416
 417 Figure 7 shows multi-year monthly mean Na⁺ concentrations in the observations (black), standard
 418 + leads simulation (orange), and standard simulation (blue) for Zeppelin (a), Utqiagvik (b), Alert
 419 (c), and Pallas (d) during the cold season for 2002-2008 (a-c) and 2003-2008 (d). We sample the
 420 model simulations in the gridbox that encompasses the latitude, longitude, and altitude of each
 421 monitoring station (see Sect. 2.3) and convert the simulated SSA to Na⁺ concentrations. For all
 422 sites and months during the cold season, the simulated and observed Na⁺ mass concentrations
 423 overlap within ± 1 standard deviation (shaded regions in Fig. 7), except in November and
 424 December at Pallas. We find mean concentrations are overpredicted in both the standard and
 425 standard + leads simulations at all sites and months during the cold season, apart from the
 426 standard model at Utqiagvik and Alert in November which agree closest with observations.
 427

428 The model overpredicts Na⁺ concentrations the most at Zeppelin and Pallas, with the standard +
429 leads and standard mean concentrations a factor of 3.2 to 4.71 and 2.0 to 4.8 higher, respectively,
430 than observations across all months during the cold season. Confer et al. (2023) similarly find an
431 overprediction of SSA at Zeppelin, which they find is exacerbated by including blowing snow
432 emissions. Additionally, Zeppelin is at high elevation (located on a mountain at 475m) and has
433 been found to be more impacted by the free troposphere and aerosol-cloud interactions than other
434 Arctic sites (Freud et al., 2017); the chemical transport model cannot represent two-way aerosol-
435 cloud interactions. The model overestimate is less at Utqiagvik, where the standard + leads
436 simulation still overpredicts observed concentrations by a factor of 1.0 to 2.4, and least at Alert,
437 with observed concentrations overestimated by a factor of 1.3 to 2.3 for the standard + leads
438 model. Lead emissions do not change the simulated seasonality of cold season surface SSA
439 concentrations. The timing of cold season maximum and minimum concentrations at Zeppelin,
440 Alert, and Pallas differs between the observed and simulated, for both the standard + leads and
441 standard models. At Utqiagvik, the maximum mass concentration in the observations and both
442 model simulations occurs in November. However, the minimum observed cold season mass
443 concentration occurs in February at Utqiagvik, whereas the standard + leads and standard mean
444 concentrations reach a minimum in April.

445
446 Figure 4a and b places the differences seen at each of the three sites in Fig. 7 into a broader
447 context, with maps of the relative and absolute increases in SSA mass concentrations for the
448 month of January. There is minimal change in SSA concentrations where Pallas is located,
449 explaining the near equal Na⁺ concentrations for the standard + leads and standard simulations
450 which results in the overlapping lines in Fig. 7d, suggesting minimal influence from leads at this
451 site likely due to its inland location. The most significant relative increase in SSA concentration
452 from leads out of the four sites occurs at Alert (Fig. 7a). However, regions with the largest changes
453 in SSA mass concentration due to leads in Fig. 4a and b for the month of January (i.e., parts of
454 Northern Canada southwest of Alert), which are consistent throughout the cold season (Fig. S-4
455 and S-5 in SI), are not sampled by long-term ground monitoring sites, which would help constrain
456 lead impacts on SSA. In our simulation, lead emissions have the same size distribution as the
457 open ocean, with most of the mass in the coarse mode (82-90%). Despite this, there are increases
458 in SSA concentration over land (Fig. 4a and b) indicating transport (see also Text S-2 and Fig.
459 S-8). This is consistent with observed inland transport of SSA across the North Slope of Alaska
460 (Simpson et al., 2005). It is likely that leads emit smaller SSA particles relative to open ocean
461 emissions (Nilsson et al., 2001), which would increase their lifetime, so non-local impacts from

Field Code Changed

Field Code Changed

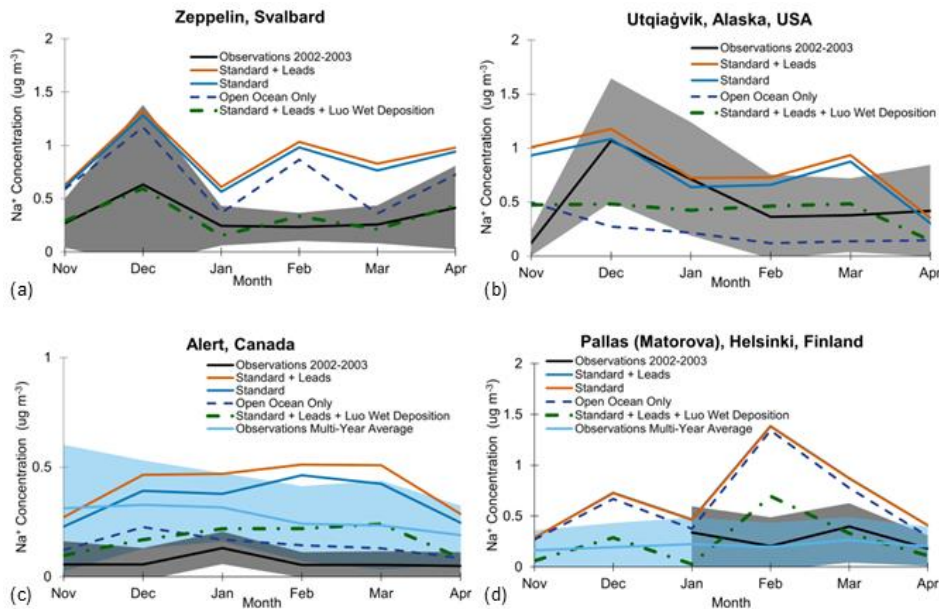
Field Code Changed

462 leads may be greater than simulated here. This further highlights the need for observations in
463 other regions to better understand the impacts of lead emissions.

464
465 There is strong observational evidence that lead emissions contribute to cold season SSA (see
466 Sect. 1), but the standard model consistently overpredicts observed SSA concentrations prior to
467 inclusion of additional lead emissions. This suggests other sources of SSA may be overpredicted
468 or sinks of SSA may be underpredicted. Ongoing work to improve the treatment of aerosol wet
469 removal processes in GEOS-Chem has not specifically investigated the impacts on sea salt
470 aerosol (Luo et al., 2020; Luo and Yu, 2023). Additionally, a recent observational study (Chen et
471 al., 2022) suggests that the GEOS-Chem blowing snow emissions parameterization may
472 overpredict the frequency of blowing snow events, therefore possibly contributing to the
473 overprediction of Arctic SSA mass concentrations.

474

Field Code Changed



475 **Figure 8-** Model evaluation for the cold season 2002-2003 at Zeppelin (a), Utqiagvik (b), Alert (c),
476 and Pallas (d). Observed Na⁺ concentrations are included as monthly averages for 2002-2003
477 (black + standard deviation margin), and the multi-year monthly averages (light blue + standard
478 deviation margin) (note: no 2002 data is available at Pallas). We show monthly average modeled
479 Na⁺ concentrations for 2002-2003 for the standard + leads (orange) and standard (blue)
480

481 simulations with two additional sensitivity studies: open ocean only emissions contributing to Na⁺
482 concentrations (dark blue with dashes) and the standard + leads emissions with Luo et al. (2020)
483 wet deposition applied (green line with dashes + dots). Note the different y-axis for Alert (c), as
484 concentrations are much lower at this site.

485

486 To test these possible sources of uncertainty, we run two additional sensitivity simulations for one
487 cold season (November 2002-April 2003): (1) using the Luo et al. (2020) wet deposition scheme
488 with the standard + leads SSA emissions (“standard + leads + Luo Wet Deposition”) and (2)
489 turning off blowing snow emissions in the standard model for an “open ocean only” case (see Text
490 S3-4 for further description). We find that the Luo wet deposition scheme improves model
491 agreement most at Zeppelin (see Fig. 8a), especially in the months of November, December,
492 March, and April. At Utqiagvik, the Luo wet deposition scheme results in underestimates in Na⁺
493 concentrations compared to observations (Fig. 8b) in December, January, and April and
494 overestimates in November, February, and March; however, the overestimated months are closer
495 to the observed concentrations than the standard + leads and standard simulations. Additionally,
496 the standard model at Utqiagvik agrees with observations in December and the standard + leads
497 model agrees with observations in January and April.

498

499 At Alert, the Luo wet deposition scheme decreases the model overestimate of the standard +
500 leads simulation when compared to the observations for the 2002-2003 cold season (Fig. 8c);
501 ~~but~~ but still overestimates Na⁺ concentrations in each month. As the 2002-2003 observations at
502 Alert are particularly low, we also include the observed multi-year (2002-2008) monthly average
503 Na⁺ concentrations for comparison. The Luo wet deposition scheme improves model evaluation
504 from February-March compared to the multi-year average observed concentrations at Alert, but
505 otherwise underpredicts concentrations. The Luo wet deposition scheme decreases
506 overprediction at Pallas in February compared to observations from the 2003 cold season and
507 improves model agreement in March and April, but underpredicts Na⁺ concentrations in January
508 (Fig. 8d). As there are no available observations in 2002 at Pallas, we also include the observed
509 multi-year (2003-2008) monthly average Na⁺ concentrations for comparison. The Luo wet
510 deposition scheme underpredicts Na⁺ concentrations in November, January, and April and
511 overpredicts concentrations in December and March compared to the multi-year average
512 concentrations at Pallas.

513

514 At Utqiaġvik, under predicted Na⁺ concentrations with only open ocean emissions (except in
515 November) suggest that this site is influenced by blowing snow emissions and/or lead emissions.
516 Of the four sites, blowing snow is most important and well-represented here, as it also improves
517 the modeled seasonality by correctly representing the December peak in Na⁺ concentrations in
518 the standard + leads and standard model; there may be larger uncertainty in the emissions
519 parameterization in other regions. At Zeppelin, Alert, and Pallas, even with open ocean emissions
520 only and the standard wet deposition, the model overestimates Na⁺ concentrations for all months
521 during the cold season for 2002-2003, except at Pallas in January, where only open ocean
522 emissions more closely match observations. Moreover, the open ocean only Na⁺ concentrations
523 are close in value to the standard + leads and standard concentrations, indicating Pallas is largely
524 influenced by open ocean emissions, rather than blowing snow and lead emissions.

525
526 The results of these sensitivity tests suggest that changes to wet scavenging may be more
527 important at higher altitudes, given the improvement in model evaluation at Zeppelin. Yet, the
528 inclusion of the Luo wet deposition scheme to the standard + leads simulation still overestimates
529 concentrations at ~~Alert,~~ and Alert and generally leads to disagreement with observations at
530 Utqiaġvik and Pallas (except in March and April at Pallas).

531

532 4. Uncertainties Discussion

533

534 Our model evaluation reveals SSA is overestimated in the standard and standard + leads model
535 at each of the 4 Arctic sampling sites, pointing to possible sources of uncertainty. First, we use
536 the Jaeglé et al. (2011) open ocean function for our lead emissions parameterization as it is the
537 standard SSA emission function in GEOS-Chem that has been previously evaluated across global
538 oceans. However, there are possible differences in the mechanisms and meteorological
539 dependencies of SSA emission from leads vs. the open ocean which could impact the magnitude
540 and spatial patterns of lead emissions. Some potential differences were investigated in a
541 summertime measurement study (Nilsson et al., 2001), where they derive an empirical lead
542 emissions flux equation with an exponential dependence on windspeed and no consideration of
543 SST (Eq. (S-2) in SI). They found the emissions rate per area from leads is smaller than that of
544 the open ocean due to lower fetch in leads, which suggests the lead emissions estimated in our
545 study may be an upper limit when considering large leads only (>3km in size); however, this lead
546 fraction detected by AMSR-E may only include 50% of total lead area (Röhrs and Kaleschke,
547 2012). Additionally, Nilsson et al. (2001) suggest leads emit smaller SSA particles relative to the

Field Code Changed

548 open ocean, which would increase their lifetime and transport distance. To create a more robust
549 understanding of the different SSA emission mechanisms from leads vs. the open ocean, more
550 studies using size-resolved observations could be conducted within the areas we predict the
551 highest lead emissions, such as within the Bering Strait, Nares Strait, Wynniatt Bay in the
552 Canadian archipelago, and the eastern Greenland Sea.

553
554 Our sensitivity study results do not ultimately confirm the source(s) of overprediction within the
555 GEOS-Chem model. Blowing snow emissions are included as a standard source of SSA
556 emissions in the Arctic, but remaining uncertainties about the GEOS-Chem blowing snow
557 emissions parameterization (Chen et al., 2022) suggest a need for refinement. ~~Additionally, t~~
558 results of the standard + leads + Luo wet deposition simulation highlight there are also remaining
559 uncertainties associated with wet deposition schemes as the Luo et al. (2020) mechanism does
560 not lead to consistent improvement of simulated SSA concentrations. Luo & Yu (2023) find that
561 the scheme overestimates wet scavenging on a global scale, so continued improvement in the
562 model deposition processes may resolve SSA overestimates. In addition, there are sparse ground
563 observations of precipitation in the Arctic, and while the MERRA-2 reanalysis uses both model
564 and satellite data to fill these gaps, Arctic cloud properties and precipitation can still be difficult to
565 predict (Barrett et al., 2020; Taylor et al., 2019), which could affect the accurate simulation of
566 aerosol deposition and, in turn, our simulated SSA concentrations.

Field Code Changed

Formatted: Font: (Default) Arial, 11 pt

567

568 5. Conclusions

569
570 Observational evidence (Chen et al., 2022; Kirpes et al., 2019; May et al., 2016; Radke et al.,
571 1976; Scott and Levin, 1972; Willis et al., 2018) and one modeling study of the 400 km² region
572 around Utqiagvik, Alaska (Ioannidis et al., 2023) have shown that leads may be an important
573 source of cold season SSA for the coastal Arctic. Here, we evaluate their importance as an Arctic-
574 wide source of cold season SSA emissions and their potential atmospheric chemistry impacts in
575 the global chemical transport model GEOS-Chem.

Field Code Changed

576
577 We find that lead SSA emissions occur primarily in regions where other SSA emissions sources
578 are very low, mainly within the Bering Strait, Nares Strait, Wynniatt Bay in the Canadian
579 archipelago, and the eastern Greenland Sea. Poleward of 75° N, leads increase total monthly
580 cold-season SSA emissions by 5.6 to 7.5%, with the highest contribution of SSA emissions from
581 leads in January and the lowest in April. Lead emissions vary in magnitude by month and year,

582 mainly due to variations in lead area. Future trends in Arctic sea ice predicted by climate models
583 suggest a possible future increasing trend in lead area (Intergovernmental Panel On Climate
584 Change, 2023), which would increase lead emissions. The additional SSA from leads in regions
585 where the background aerosol concentrations are low could also affect local aerosol-cloud
586 interactions, but the overall warming or cooling effect of these additional aerosols remains
587 uncertain (Cox et al., 2015; Schmale et al., 2021; Stramler et al., 2011; Tan et al., 2023; Villanueva
588 et al., 2022).

589
590 SSA mass concentrations increase primarily at the location of lead emissions, in regions where
591 the standard SSA mass concentration is very low ($\leq 1.2 \mu\text{g m}^{-3}$). Throughout the cold season, the
592 increased SSA mass concentrations from leads remain relatively constant in magnitude and
593 spatial distribution. The highest increase in multi-year average SSA mass concentrations due to
594 leads, spatially averaged for $\geq 75^\circ\text{N}$, occurs in November ($5.7\% \pm 5.2\%$) and the lowest occurs in
595 April ($3.7\% \pm 2.9\%$). Increased SSA from leads increases surface Br concentrations during the
596 cold season in corresponding locations. We find total Arctic-wide ($\geq 60^\circ\text{N}$) increases in multi-year
597 mean surface Br concentration range from 2.8 to 8.8%. The increases in Br are not sufficient to
598 have an impact on ozone; subsequent decreases in average surface ozone concentrations in the
599 Arctic are negligible ($< -0.25\%$).

600
601 Overall, we predict sea ice leads may impact Arctic-wide cold-season SSA concentrations and Br
602 concentrations by up to 5-10% on average during the 2002-2008 period. As leads are likely to
603 increase in prevalence under climate change, including this source of SSA in chemistry and
604 climate models may become more important for future predictions.

605
606 **Code and Data Availability**
607 Standard model code: <https://doi.org/10.5281/zenodo.5500717>; AMSR-E data:
608 <https://www.cen.uni-hamburg.de/en/icdc/data/cryosphere/lead-area-fraction-amsre.html>);
609 observational site data (Alert, Pallas, and Zeppelin): <https://ebas-data.nilu.no/Default.aspx>;
610 observational data (Utqiaġvik): <https://saga.pmel.noaa.gov/data/stations/>; model data shown in
611 paper: <https://doi.org/10.5281/zenodo.14611355>.

612
613 **Author Contribution**

614 EJE was responsible for data curation, model simulations, validation, visualization, and analysis
615 with expert advice from HMM. HMM is responsible for conceptualization. EJE drafted the
616 manuscript which was revised by HMM.

617

618 **Competing Interests**

619 The authors declare that they have no conflict of interest.

620

621 **Acknowledgements**

622 We thank Kerri Pratt for helpful discussions. HMM was supported by Department of Energy (DOE)
623 Atmospheric Systems Research (ASR), award DE-SC0023049. We acknowledge financial
624 support from the department of Civil and Environmental Engineering at the University of Illinois
625 Urbana-Champaign.

626

627 **Supplemental Information**

628 Equations of SSA flux from Jaegle et al. (2011) and Nilsson et al. (2001); Additional figures of lead
629 SSA emissions for months other than January during the cold season; Cold season total lead
630 SSA emissions; Description and figure of the correlation between lead area and lead SSA
631 emissions; long-term trends in lead area (2002-2011) and relevant statistical testing; additional
632 figures of multi-year (2002-2008) mean percent increase due to leads in SSA and bromine
633 concentration for months other than January during the cold season; Description and figures of
634 correlation between lead emissions and coarse and accumulation mode SSA concentration;
635 Sensitivity simulations.

636

637 **6. References**

638

639 [Abbatt, J. P. D., Thomas, J. L., Abrahamsson, K., Boxe, C., Granfors, A., Jones, A. E., King, M. D., Saiz-Lopez, A., Shepson, P. B., Sodeau, J., Toohey, D. W., Toubin, C., Von Glasow, R., Wren, S. N., and Yang, X.: Halogen activation via interactions with environmental ice and snow in the polar lower troposphere and other regions, *Atmospheric Chem. Phys.*, **12**, 6237–6271, <https://doi.org/10.5194/acp-12-6237-2012>, 2012.](#)

643 [Alvarez-Aviles, L., Simpson, W. R., Douglas, T. A., Sturm, M., Perovich, D., and Domine, F.: Frost flower chemical composition during growth and its implications for aerosol production and bromine activation, *J. Geophys. Res. Atmospheres*, **113**, 2008JD010277, <https://doi.org/10.1029/2008JD010277>, 2008.](#)

646 [Amos, H. M., Jacob, D. J., Holmes, C. D., Fisher, J. A., Wang, Q., Yantosca, R. M., Corbitt, E. S., Galarneau, E., Rutter, A. P., Gustin, M. S., Steffen, A., Schauer, J. J., Graydon, J. A., Louis, V. L. St., Talbot, R. W., Edgerton, E. S., Zhang, Y., and Sunderland, E. M.: Gas-particle partitioning of atmospheric Hg\(II\) and its effect on global mercury deposition, *Atmospheric Chem. Phys.*, **12**, 591–603, <https://doi.org/10.5194/acp-12-591-2012>, 2012.](#)

650
26

Formatted: Bibliography, Widow/Orphan control, Adjust space between Latin and Asian text, Adjust space between Asian text and numbers

651 [Barrett, A. P., Stroeve, J. C., and Serreze, M. C.: Arctic Ocean Precipitation From Atmospheric Reanalyses](#)
652 [and Comparisons With North Pole Drifting Station Records, *J. Geophys. Res. Oceans*, 125,](#)
653 [e2019JC015415, <https://doi.org/10.1029/2019JC015415>, 2020.](#)

654 [Chen, Q., Mirrielees, J. A., Thanekar, S., Loeb, N. A., Kirpes, R. M., Upchurch, L. M., Barget, A. J., Lata, N.](#)
655 [N., Raso, A. R. W., McNamara, S. M., China, S., Quinn, P. K., Ault, A. P., Kennedy, A., Shepson, P. B.,](#)
656 [Fuentes, J. D., and Pratt, K. A.: Atmospheric particle abundance and sea salt aerosol observations in the](#)
657 [springtime Arctic: a focus on blowing snow and leads, *Atmospheric Chem. Phys.*, 22, 15263–15285,](#)
658 [https://doi.org/10.5194/acp-22-15263-2022, 2022.](#)

659 [Confer, K. L., Jaeglé, L., Liston, G. E., Sharma, S., Nandan, V., Yackel, J., Ewert, M., and Horowitz, H. M.:](#)
660 [Impact of Changing Arctic Sea Ice Extent, Sea Ice Age, and Snow Depth on Sea Salt Aerosol From Blowing](#)
661 [Snow and the Open Ocean for 1980–2017, *J. Geophys. Res. Atmospheres*, 128, e2022JD037667,](#)
662 [https://doi.org/10.1029/2022JD037667, 2023.](#)

663 [Cox, C. J., Walden, V. P., Rowe, P. M., and Shupe, M. D.: Humidity trends imply increased sensitivity to](#)
664 [clouds in a warming Arctic, *Nat. Commun.*, 6, 10117, <https://doi.org/10.1038/ncomms10117>, 2015.](#)

665 [DeMott, P. J., Hill, T. C. J., McCluskey, C. S., Prather, K. A., Collins, D. B., Sullivan, R. C., Ruppel, M. J.,](#)
666 [Mason, R. H., Irish, V. E., Lee, T., Hwang, C. Y., Rhee, T. S., Snider, J. R., McMeeking, G. R., Dhaniyala, S.,](#)
667 [Lewis, E. R., Wentzell, J. J. B., Abbatt, J., Lee, C., Sultana, C. M., Ault, A. P., Axson, J. L., Diaz Martinez, M.,](#)
668 [Venero, I., Santos-Figueroa, G., Stokes, M. D., Deane, G. B., Mayol-Bracero, O. L., Grassian, V. H., Bertram,](#)
669 [T. H., Bertram, A. K., Moffett, B. F., and Franc, G. D.: Sea spray aerosol as a unique source of ice](#)
670 [nucleating particles, *Proc. Natl. Acad. Sci.*, 113, 5797–5803, <https://doi.org/10.1073/pnas.1514034112>,](#)
671 [2016.](#)

672 [Dibb, J. E., Ziemba, L. D., Luxford, J., and Beckman, P.: Bromide and other ions in the snow, firn air, and](#)
673 [atmospheric boundary layer at Summit during GSHOX, *Atmospheric Chem. Phys.*, 10, 9931–9942,](#)
674 [https://doi.org/10.5194/acp-10-9931-2010, 2010.](#)

675 [Domine, F., Sparapani, R., Ianniello, A., and Beine, H. J.: The origin of sea salt in snow on Arctic sea ice](#)
676 [and in coastal regions, *Atmospheric Chem. Phys.*, 4, 2259–2271, \[https://doi.org/10.5194/acp-4-2259-\]\(https://doi.org/10.5194/acp-4-2259-2004\)](#)
677 [2004, 2004.](#)

678 [Freud, E., Krejci, R., Tunved, P., Leaitch, R., Nguyen, Q. T., Massling, A., Skov, H., and Barrie, L.: Pan-Arctic](#)
679 [aerosol number size distributions: seasonality and transport patterns, *Atmospheric Chem. Phys.*, 17,](#)
680 [8101–8128, <https://doi.org/10.5194/acp-17-8101-2017>, 2017.](#)

681 [Gelaro, R., McCarty, W., Suárez, M. J., Todling, R., Molod, A., Takacs, L., Randles, C. A., Darmenov, A.,](#)
682 [Bosilovich, M. G., Reichle, R., Wargan, K., Coy, L., Cullather, R., Draper, C., Akella, S., Buchard, V., Conaty,](#)
683 [A., Da Silva, A. M., Gu, W., Kim, G.-K., Koster, R., Lucchesi, R., Merkova, D., Nielsen, J. E., Partyka, G.,](#)
684 [Pawson, S., Putman, W., Rienecker, M., Schubert, S. D., Sienkiewicz, M., and Zhao, B.: The Modern-Era](#)
685 [Retrospective Analysis for Research and Applications, Version 2 \(MERRA-2\), *J. Clim.*, 30, 5419–5454,](#)
686 [https://doi.org/10.1175/JCLI-D-16-0758.1, 2017.](#)

687 [Gong, S. L.: A parameterization of sea-salt aerosol source function for sub- and super-micron particles,](#)
688 [*Glob. Biogeochem. Cycles*, 17, 2003GB002079, <https://doi.org/10.1029/2003GB002079>, 2003.](#)

689 [Huang, J. and Jaeglé, L.: Wintertime enhancements of sea salt aerosol in polar regions consistent with a](#)
690 [sea ice source from blowing snow, *Atmospheric Chem. Phys.*, **17**, 3699–3712,](#)
691 <https://doi.org/10.5194/acp-17-3699-2017>, 2017.

692 [Huang, J., Jaeglé, L., and Shah, V.: Using CALIOP to constrain blowing snow emissions of sea salt aerosols](#)
693 [over Arctic and Antarctic sea ice, *Atmospheric Chem. Phys.*, **18**, 16253–16269,](#)
694 <https://doi.org/10.5194/acp-18-16253-2018>, 2018.

695 [Huang, J., Jaeglé, L., Chen, Q., Alexander, B., Sherwen, T., Evans, M. J., Theys, N., and Choi, S.: Evaluating](#)
696 [the impact of blowing-snow sea salt aerosol on springtime BrO and O₃ in the](#)
697 [Arctic, *Atmospheric Chem. Phys.*, **20**, 7335–7358, <https://doi.org/10.5194/acp-20-7335-2020>, 2020.](#)

698 [Integrated Climate Data Center \(ICDC\), CEN, and University of Hamburg, Hamburg, Germany: AMSR-E](#)
699 [Arctic lead area fraction, n.d.](#)

700 [Intergovernmental Panel On Climate Change: Climate Change 2021 – The Physical Science Basis: Working](#)
701 [Group I Contribution to the Sixth Assessment Report of the Intergovernmental Panel on Climate Change,](#)
702 [1st ed., Cambridge University Press, <https://doi.org/10.1017/9781009157896>, 2023.](#)

703 [Ioannidis, E., Law, K. S., Raut, J.-C., Marelle, L., Onishi, T., Kirpes, R. M., Upchurch, L. M., Tuch, T.,](#)
704 [Wiedensohler, A., Massling, A., Skov, H., Quinn, P. K., and Pratt, K. A.: Modelling wintertime sea-spray](#)
705 [aerosols under Arctic haze conditions, *Atmospheric Chem. Phys.*, **23**, 5641–5678,](#)
706 <https://doi.org/10.5194/acp-23-5641-2023>, 2023.

707 [Jaeglé, L., Quinn, P. K., Bates, T. S., Alexander, B., and Lin, J.-T.: Global distribution of sea salt aerosols:](#)
708 [new constraints from in situ and remote sensing observations, *Atmospheric Chem. Phys.*, **11**, 3137–3157,](#)
709 <https://doi.org/10.5194/acp-11-3137-2011>, 2011.

710 [Keller, C. A., Long, M. S., Yantosca, R. M., Da Silva, A. M., Pawson, S., and Jacob, D. J.: HEMCO v1.0: a](#)
711 [versatile, ESMF-compliant component for calculating emissions in atmospheric models, *Geosci. Model*](#)
712 [Dev., **7**, 1409–1417, <https://doi.org/10.5194/gmd-7-1409-2014>, 2014.](#)

713 [Kirpes, R. M., Bonanno, D., May, N. W., Fraund, M., Barget, A. J., Moffet, R. C., Ault, A. P., and Pratt, K. A.:](#)
714 [Wintertime Arctic Sea Spray Aerosol Composition Controlled by Sea Ice Lead Microbiology, *ACS Cent.*](#)
715 [Sci., **5**, 1760–1767, <https://doi.org/10.1021/acscentsci.9b00541>, 2019.](#)

716 [Leaitch, W. R., Russell, L. M., Liu, J., Kolonjari, F., Toom, D., Huang, L., Sharma, S., Chivulescu, A., Veber,](#)
717 [D., and Zhang, W.: Organic functional groups in the submicron aerosol at 82.5° N, 62.5° W from 2012 to](#)
718 [2014, *Atmospheric Chem. Phys.*, **18**, 3269–3287, <https://doi.org/10.5194/acp-18-3269-2018>, 2018.](#)

719 [Lin, H., Jacob, D. J., Lundgren, E. W., Sulprizio, M. P., Keller, C. A., Fritz, T. M., Eastham, S. D., Emmons, L.](#)
720 [K., Campbell, P. C., Baker, B., Saylor, R. D., and Montuoro, R.: Harmonized Emissions Component](#)
721 [\(HEMCO\) 3.0 as a versatile emissions component for atmospheric models: application in the GEOS-](#)
722 [Chem, NASA GEOS, WRF-GC, CESM2, NOAA GEFS-Aerosol, and NOAA UFS models, *Geosci. Model Dev.*,](#)
723 [14, 5487–5506, <https://doi.org/10.5194/gmd-14-5487-2021>, 2021.](#)

724 [Liu, H., Jacob, D. J., Bey, I., and Yantosca, R. M.: Constraints from ²¹⁰Pb and ⁷Be on wet deposition and](#)
725 [transport in a global three-dimensional chemical tracer model driven by assimilated meteorological](#)
726 [fields, *J. Geophys. Res. Atmospheres*, **106**, 12109–12128, <https://doi.org/10.1029/2000JD900839>, 2001.](#)

727 [Luo, G. and Yu, F.: Impact of Air Refreshing and Cloud Ice Uptake Limitations on Vertical Profiles and Wet](#)
728 [Depositions of Nitrate, Ammonium, and Sulfate, *Geophys. Res. Lett.*, 50, e2023GL104258,](#)
729 <https://doi.org/10.1029/2023GL104258>, 2023.

730 [Luo, G., Yu, F., and Moch, J. M.: Further improvement of wet process treatments in GEOS-Chem v12.6.0:](#)
731 [impact on global distributions of aerosols and aerosol precursors, *Geosci. Model Dev.*, 13, 2879–2903,](#)
732 <https://doi.org/10.5194/gmd-13-2879-2020>, 2020.

733 [May, N. W., Quinn, P. K., McNamara, S. M., and Pratt, K. A.: Multiyear study of the dependence of sea salt](#)
734 [aerosol on wind speed and sea ice conditions in the coastal Arctic, *J. Geophys. Res. Atmospheres*, 121,](#)
735 [9208–9219, https://doi.org/10.1002/2016JD025273](https://doi.org/10.1002/2016JD025273), 2016.

736 [Monahan, E. C., Spiel, D. E., and Davidson, K. L.: A Model of Marine Aerosol Generation Via Whitecaps](#)
737 [and Wave Disruption, in: *Oceanic Whitecaps*, vol. 2, edited by: Monahan, E. C. and Niocaill, G. M.,](#)
738 [Springer Netherlands, Dordrecht, 167–174, https://doi.org/10.1007/978-94-009-4668-2_16](#), 1986.

739 [Nilsson, E. D., Rannik, Ü., Swietlicki, E., Leck, C., Aalto, P. P., Zhou, J., and Norman, M.: Turbulent aerosol](#)
740 [fluxes over the Arctic Ocean: 2. Wind-driven sources from the sea, *J. Geophys. Res. Atmospheres*, 106,](#)
741 [32139–32154, https://doi.org/10.1029/2000JD900747](https://doi.org/10.1029/2000JD900747), 2001.

742 [Pierce, J. R. and Adams, P. J.: Global evaluation of CCN formation by direct emission of sea salt and](#)
743 [growth of ultrafine sea salt, *J. Geophys. Res. Atmospheres*, 111, 2005JD006186,](#)
744 <https://doi.org/10.1029/2005JD006186>, 2006.

745 [Pound, R. J., Sherwen, T., Helmig, D., Carpenter, L. J., and Evans, M. J.: Influences of oceanic ozone](#)
746 [deposition on tropospheric photochemistry, *Atmospheric Chem. Phys.*, 20, 4227–4239,](#)
747 <https://doi.org/10.5194/acp-20-4227-2020>, 2020.

748 [Pratt, K. A., Custard, K. D., Shepson, P. B., Douglas, T. A., Pöhler, D., General, S., Zielcke, J., Simpson, W. R.,](#)
749 [Platt, U., Tanner, D. J., Gregory Huey, L., Carlsen, M., and Stirm, B. H.: Photochemical production of](#)
750 [molecular bromine in Arctic surface snowpacks, *Nat. Geosci.*, 6, 351–356,](#)
751 <https://doi.org/10.1038/ngeo1779>, 2013.

752 [Quinn, P. K., Coffman, D. J., Kapustin, V. N., Bates, T. S., and Covert, D. S.: Aerosol optical properties in the](#)
753 [marine boundary layer during the First Aerosol Characterization Experiment \(ACE 1\) and the underlying](#)
754 [chemical and physical aerosol properties, *J. Geophys. Res.*, 103, 16,547–16,563](#), 1998.

755 [Quinn, P. K., Bates, T. S., Miller, T. L., Coffman, D. J., Johnson, J. E., Harris, J. M., Ogren, J. A., Forbes, G.,](#)
756 [Anderson, T. L., Covert, D. S., and Rood, M. J.: Surface submicron aerosol chemical composition: What](#)
757 [fraction is not sulfate?, *J. Geophys. Res. Atmospheres*, 105, 6785–6805,](#)
758 <https://doi.org/10.1029/1999JD901034>, 2000.

759 [Quinn, P. K., Miller, T. L., Bates, T. S., Ogren, J. A., Andrews, E., and Shaw, G. E.: A 3-year record of](#)
760 [simultaneously measured aerosol chemical and optical properties at Barrow, Alaska, *J. Geophys. Res.*](#)
761 [Atmospheres](#), 107, <https://doi.org/10.1029/2001JD001248>, 2002.

762 [Radke, L. F., Hobbs, P. V., and Pinnons, J. E.: Observations of Cloud Condensation Nuclei, Sodium-](#)
763 [Containing Particles, Ice Nuclei and the Light-Scattering Coefficient Near Barrow, Alaska, *J. Appl. Meteor.*](#)

764 [Climatol.](https://doi.org/10.1175/1520-0450(1976)015%3C0982:OCCNS%3E2.0.CO;2), 15, 982–995, [https://doi.org/10.1175/1520-0450\(1976\)015%3C0982:OCCNS%3E2.0.CO;2](https://doi.org/10.1175/1520-0450(1976)015%3C0982:OCCNS%3E2.0.CO;2),
765 [1976](https://doi.org/10.1175/1520-0450(1976)015%3C0982:OCCNS%3E2.0.CO;2).

766 Rhodes, R. H., Yang, X., Wolff, E. W., McConnell, J. R., and Frey, M. M.: Sea ice as a source of sea salt
767 aerosol to Greenland ice cores: a model-based study, *Atmospheric Chem. Phys.*, 17, 9417–9433,
768 <https://doi.org/10.5194/acp-17-9417-2017>, 2017.

769 Riley, J. P. and Chester, R.: Introduction to marine chemistry, Academic Press, London, New York, 465 pp.,
770 [1971](https://doi.org/10.1016/B978-0-12-088401-0).

771 Röhrs, J. and Kaleschke, L.: An algorithm to detect sea ice leads by using AMSR-E passive microwave
772 imagery, *The Cryosphere*, 6, 343–352, <https://doi.org/10.5194/tc-6-343-2012>, 2012.

773 Roscoe, H. K., Brooks, B., Jackson, A. V., Smith, M. H., Walker, S. J., Obbard, R. W., and Wolff, E. W.: Frost
774 flowers in the laboratory: Growth, characteristics, aerosol, and the underlying sea ice, *J. Geophys. Res.*,
775 116, D12301, <https://doi.org/10.1029/2010JD015144>, 2011.

776 Salmi, T.: Measurement of Inorganics in air and particle phase at Pallas (Matorova) (3),
777 <https://doi.org/10.48597/T6MX-CEKH>, 2018.

778 Schmale, J., Zieger, P., and Ekman, A. M. L.: Aerosols in current and future Arctic climate, *Nat. Clim.*
779 *Change*, 11, 95–105, <https://doi.org/10.1038/s41558-020-00969-5>, 2021.

780 Scott, W. D. and Levin, Z.: Open Channels in Sea Ice (Leads) as Ion Sources, *Science*, 177, 425–426,
781 <https://doi.org/10.1126/science.177.4047.425>, 1972.

782 Screen, J. A. and Simmonds, I.: Declining summer snowfall in the Arctic: causes, impacts and feedbacks,
783 *Clim. Dyn.*, 38, 2243–2256, <https://doi.org/10.1007/s00382-011-1105-2>, 2012.

784 Simpson, W. R., Alvarez-Aviles, L., Douglas, T. A., Sturm, M., and Domine, F.: Halogens in the coastal snow
785 pack near Barrow, Alaska: Evidence for active bromine air-snow chemistry during springtime, *Geophys.*
786 *Res. Lett.*, 32, 2004GL021748, <https://doi.org/10.1029/2004GL021748>, 2005.

787 Simpson, W. R., Von Glasow, R., Riedel, K., Anderson, P., Ariya, P., Bottenheim, J., Burrows, J., Carpenter,
788 L. J., Frieß, U., Goodsite, M. E., Heard, D., Hutterli, M., Jacobi, H.-W., Kaleschke, L., Neff, B., Plane, J., Platt,
789 U., Richter, A., Roscoe, H., Sander, R., Shepson, P., Sodeau, J., Steffen, A., Wagner, T., and Wolff, E.:
790 Halogens and their role in polar boundary-layer ozone depletion, *Atmospheric Chem. Phys.*, 7, 4375–
791 4418, <https://doi.org/10.5194/acp-7-4375-2007>, 2007.

792 Stramler, K., Del Genio, A. D., and Rossow, W. B.: Synoptically Driven Arctic Winter States, *J. Clim.*, 24,
793 1747–1762, <https://doi.org/10.1175/2010JCLI3817.1>, 2011.

794 Stutz, J., Thomas, J. L., Hurlock, S. C., Schneider, M., Von Glasow, R., Piot, M., Gorham, K., Burkhart, J. F.,
795 Ziemba, L., Dibb, J. E., and Lefer, B. L.: Longpath DOAS observations of surface BrO at Summit, Greenland,
796 *Atmospheric Chem. Phys.*, 11, 9899–9910, <https://doi.org/10.5194/acp-11-9899-2011>, 2011.

797 Sumata, H., De Steur, L., Divine, D. V., Granskog, M. A., and Gerland, S.: Regime shift in Arctic Ocean sea
798 ice thickness, *Nature*, 615, 443–449, <https://doi.org/10.1038/s41586-022-05686-x>, 2023.

799 [Swanson, W. F., Holmes, C. D., Simpson, W. R., Confer, K., Marelle, L., Thomas, J. L., Jaeglé, L., Alexander,](#)
800 [B., Zhai, S., Chen, Q., Wang, X., and Sherwen, T.: Comparison of model and ground observations finds](#)
801 [snowpack and blowing snow aerosols both contribute to Arctic tropospheric reactive bromine,](#)
802 [Atmospheric Chem. Phys., 22, 14467–14488, <https://doi.org/10.5194/acp-22-14467-2022>, 2022.](#)

803 [Tan, I., Sotiropoulou, G., Taylor, P. C., Zamora, L., and Wendisch, M.: A Review of the Factors Influencing](#)
804 [Arctic Mixed-Phase Clouds: Progress and Outlook, in: Geophysical Monograph Series, edited by: Sullivan,](#)
805 [S. C. and Hoose, C., Wiley, 103–132, <https://doi.org/10.1002/9781119700357.ch5>, 2023.](#)

806 [Taylor, P. C., Boeke, R. C., Li, Y., and Thompson, D. W. J.: Arctic cloud annual cycle biases in climate](#)
807 [models, Atmospheric Chem. Phys., 19, 8759–8782, <https://doi.org/10.5194/acp-19-8759-2019>, 2019.](#)

808 [Vaughan, D., Comiso, J., Allison, I., Carrasco, J., Kaser, G., Kwok, R., Mote, P., Murray, T., Paul, F., Ren, J. F.,](#)
809 [Rignot, E., Solomina, O., Steffen, K., and Zhang, T.: Observations: Cryosphere, in: Climate Change 2013:](#)
810 [The Physical Science Basis, 317–382, 2013.](#)

811 [Villanueva, D., Possner, A., Neubauer, D., Gasparini, B., Lohmann, U., and Tesche, M.: Mixed-phase](#)
812 [regime cloud thinning could help restore sea ice, Environ. Res. Lett., 17, 114057,](#)
813 <https://doi.org/10.1088/1748-9326/aca16d>, 2022.

814 [Wang, Q., Jacob, D. J., Spackman, J. R., Perring, A. E., Schwarz, J. P., Moteki, N., Marais, E. A., Ge, C.,](#)
815 [Wang, J., and Barrett, S. R. H.: Global budget and radiative forcing of black carbon aerosol: Constraints](#)
816 [from pole-to-pole \(HIPPO\) observations across the Pacific, J. Geophys. Res. Atmospheres, 119, 195–206,](#)
817 <https://doi.org/10.1002/2013JD020824>, 2014.

818 [Wang, X., Jacob, D. J., Downs, W., Zhai, S., Zhu, L., Shah, V., Holmes, C. D., Sherwen, T., Alexander, B.,](#)
819 [Evans, M. J., Eastham, S. D., Neuman, J. A., Veres, P. R., Koenig, T. K., Volkamer, R., Huey, L. G., Bannan, T.](#)
820 [J., Percival, C. J., Lee, B. H., and Thornton, J. A.: Global tropospheric halogen \(Cl, Br, I\) chemistry and its](#)
821 [impact on oxidants, Atmospheric Chem. Phys., 21, 13973–13996, \[https://doi.org/10.5194/acp-21-13973-\]\(https://doi.org/10.5194/acp-21-13973-2021\)](#)
822 [2021](#), 2021.

823 [Wang, Y., Jacob, D. J., and Logan, J. A.: Global simulation of tropospheric O₃-NO_x-hydrocarbon](#)
824 [chemistry: 3. Origin of tropospheric ozone and effects of nonmethane hydrocarbons, J. Geophys. Res.](#)
825 [Atmospheres, 103, 10757–10767, <https://doi.org/10.1029/98JD00156>, 1998.](#)

826 [Willis, M. D., Leitch, W. R., and Abbatt, J. P. D.: Processes Controlling the Composition and Abundance of](#)
827 [Arctic Aerosol, Rev. Geophys., 56, 621–671, <https://doi.org/10.1029/2018RG000602>, 2018.](#)

828 [World Meteorological Organization \(WMO\): WMO/GAW aerosol measurement procedures, guidelines](#)
829 [and recommendations, WMO, Geneva, 2003.](#)

830 [Yang, X., Neděla, V., Runštuk, J., Ondrušková, G., Krausko, J., Vetráková, Ľ., and Heger, D.: Evaporating](#)
831 [brine from frost flowers with electron microscopy and implications for atmospheric chemistry and sea-](#)
832 [salt aerosol formation, Atmospheric Chem. Phys., 17, 6291–6303, \[https://doi.org/10.5194/acp-17-6291-\]\(https://doi.org/10.5194/acp-17-6291-2017\)](#)
833 [2017](#), 2017.

834 [Zhang, L., Gong, S., Padro, J., and Barrie, L.: A size-segregated particle dry deposition scheme for an](#)
835 [atmospheric aerosol module, Atmos. Environ., 35, 549–560, 2001.](#)

836 Abbatt, J. P. D., Thomas, J. L., Abrahamsson, K., Boxe, C., Granfors, A., Jones, A. E., King, M. D., Saiz-Lopez,
837 A., Shepson, P. B., Sodeau, J., Toohey, D. W., Toubin, C., Von Glasow, R., Wren, S. N., and Yang, X.: Halogen
838 activation via interactions with environmental ice and snow in the polar lower troposphere and other
839 regions, *Atmospheric Chem. Phys.*, *12*, 6237–6271, <https://doi.org/10.5194/acp-12-6237-2012>, 2012.

840 Alvarez-Aviles, L., Simpson, W. R., Douglas, T. A., Sturm, M., Perovich, D., and Domine, F.: Frost flower
841 chemical composition during growth and its implications for aerosol production and bromine activation,
842 *J. Geophys. Res. Atmospheres*, *113*, 2008JD010277, <https://doi.org/10.1029/2008JD010277>, 2008.

843 Amos, H. M., Jacob, D. J., Holmes, C. D., Fisher, J. A., Wang, Q., Yantosca, R. M., Corbitt, E. S., Galarneau,
844 E., Rutter, A. P., Gustin, M. S., Steffen, A., Schauer, J. J., Graydon, J. A., Louis, V. L. St., Talbot, R. W.,
845 Edgerton, E. S., Zhang, Y., and Sunderland, E. M.: Gas-particle partitioning of atmospheric Hg(II) and its
846 effect on global mercury deposition, *Atmospheric Chem. Phys.*, *12*, 591–603,
847 <https://doi.org/10.5194/acp-12-591-2012>, 2012.

848 Chen, Q., Mirrielees, J. A., Thanekar, S., Loeb, N. A., Kirpes, R. M., Upchurch, L. M., Barget, A. J., Lata, N.,
849 N., Raso, A. R. W., McNamara, S. M., China, S., Quinn, P. K., Ault, A. P., Kennedy, A., Shepson, P. B.,
850 Fuentes, J. D., and Pratt, K. A.: Atmospheric particle abundance and sea-salt aerosol observations in the
851 springtime Arctic: a focus on blowing snow and leads, *Atmospheric Chem. Phys.*, *22*, 15263–15285,
852 <https://doi.org/10.5194/acp-22-15263-2022>, 2022.

853 Confer, K. L., Jaeglé, L., Liston, G. E., Sharma, S., Nandan, V., Yackel, J., Ewert, M., and Horowitz, H. M.:
854 Impact of Changing Arctic Sea-Ice Extent, Sea-Ice Age, and Snow Depth on Sea-Salt Aerosol From Blowing
855 Snow and the Open Ocean for 1980–2017, *J. Geophys. Res. Atmospheres*, *128*, e2022JD037667,
856 <https://doi.org/10.1029/2022JD037667>, 2023.

857 Cox, C. J., Walden, V. P., Rowe, P. M., and Shupe, M. D.: Humidity trends imply increased sensitivity to
858 clouds in a warming Arctic, *Nat. Commun.*, *6*, 10117, <https://doi.org/10.1038/ncomms10117>, 2015.

859 DeMott, P. J., Hill, T. C. J., McCluskey, C. S., Prather, K. A., Collins, D. B., Sullivan, R. C., Ruppel, M. J.,
860 Mason, R. H., Irish, V. E., Lee, T., Hwang, C. Y., Rhee, T. S., Snider, J. R., McMeeking, G. R., Dhaniyala, S.,
861 Lewis, E. R., Wentzell, J. J. B., Abbatt, J., Lee, C., Sultana, C. M., Ault, A. P., Axson, J. L., Diaz-Martinez, M.,
862 Venero, I., Santos-Figueroa, G., Stokes, M. D., Deane, G. B., Mayol-Bracero, O. L., Grassian, V. H., Bertram,
863 T. H., Bertram, A. K., Moffett, B. F., and Franc, G. D.: Sea-spray aerosol as a unique source of ice
864 nucleating particles, *Proc. Natl. Acad. Sci.*, *113*, 5797–5803, <https://doi.org/10.1073/pnas.1514034112>,
865 2016.

866 Dibb, J. E., Ziemba, L. D., Luxford, J., and Beckman, P.: Bromide and other ions in the snow, firn air, and
867 atmospheric boundary layer at Summit during GSHOX, *Atmospheric Chem. Phys.*, *10*, 9931–9942,
868 <https://doi.org/10.5194/acp-10-9931-2010>, 2010.

869 Domine, F., Sparapani, R., Ianniello, A., and Beine, H. J.: The origin of sea salt in snow on Arctic sea-ice
870 and in coastal regions, *Atmospheric Chem. Phys.*, *4*, 2259–2271, [https://doi.org/10.5194/acp-4-2259-](https://doi.org/10.5194/acp-4-2259-2004)
871 2004, 2004.

872 Freud, E., Krejci, R., Tunved, P., Leaitch, R., Nguyen, Q. T., Massling, A., Skov, H., and Barrie, L.: Pan-Arctic
873 aerosol number size distributions: seasonality and transport patterns, *Atmospheric Chem. Phys.*, *17*,
874 8101–8128, <https://doi.org/10.5194/acp-17-8101-2017>, 2017.

875 Gelaro, R., McCarty, W., Suárez, M. J., Todling, R., Molod, A., Takacs, L., Randles, C. A., Darmenov, A.,
876 Bosilovich, M. G., Reichle, R., Wargan, K., Coy, L., Cullather, R., Draper, C., Akella, S., Buchard, V., Conaty,
877 A., Da Silva, A. M., Gu, W., Kim, G. K., Koster, R., Lucchesi, R., Merkova, D., Nielsen, J. E., Partyka, G.,
878 Pawson, S., Putman, W., Rienecker, M., Schubert, S. D., Sienkiewicz, M., and Zhao, B.: The Modern-Era
879 Retrospective Analysis for Research and Applications, Version 2 (MERRA-2), *J. Clim.*, **30**, 5419–5454,
880 <https://doi.org/10.1175/JCLI-D-16-0758.1>, 2017.

881 Gong, S.-L.: A parameterization of sea-salt aerosol source function for sub- and super-micron particles,
882 *Glob. Biogeochem. Cycles*, **17**, 2003GB002079, <https://doi.org/10.1029/2003GB002079>, 2003.

883 Huang, J. and Jaeglé, L.: Wintertime enhancements of sea salt aerosol in polar regions consistent with a
884 sea-ice source from blowing snow, *Atmospheric Chem. Phys.*, **17**, 3699–3712,
885 <https://doi.org/10.5194/acp-17-3699-2017>, 2017.

886 Huang, J., Jaeglé, L., and Shah, V.: Using CALIOP to constrain blowing snow emissions of sea salt aerosols
887 over Arctic and Antarctic sea ice, *Atmospheric Chem. Phys.*, **18**, 16253–16269,
888 <https://doi.org/10.5194/acp-18-16253-2018>, 2018.

889 Huang, J., Jaeglé, L., Chen, Q., Alexander, B., Sherwen, T., Evans, M. J., Theys, N., and Choi, S.: Evaluating
890 the impact of blowing snow sea salt aerosol on springtime BrO and O₃ in the
891 Arctic, *Atmospheric Chem. Phys.*, **20**, 7335–7358, <https://doi.org/10.5194/acp-20-7335-2020>, 2020.

892 Integrated Climate Data Center (ICDC), CEN, and University of Hamburg, Hamburg, Germany: AMSR-E
893 Arctic lead area fraction, n.d.

894 Intergovernmental Panel On Climate Change: Climate Change 2021 – The Physical Science Basis: Working
895 Group I Contribution to the Sixth Assessment Report of the Intergovernmental Panel on Climate Change,
896 1st ed., Cambridge University Press, <https://doi.org/10.1017/9781009157896>, 2023.

897 Ioannidis, E., Law, K. S., Raut, J. C., Marelle, L., Onishi, T., Kirpes, R. M., Upchurch, L. M., Tuch, T.,
898 Wiedensohler, A., Massling, A., Skov, H., Quinn, P. K., and Pratt, K. A.: Modelling wintertime sea-spray
899 aerosols under Arctic haze conditions, *Atmospheric Chem. Phys.*, **23**, 5641–5678,
900 <https://doi.org/10.5194/acp-23-5641-2023>, 2023.

901 Jaeglé, L., Quinn, P. K., Bates, T. S., Alexander, B., and Lin, J.-T.: Global distribution of sea-salt aerosols:
902 new constraints from in-situ and remote sensing observations, *Atmospheric Chem. Phys.*, **11**, 3137–3157,
903 <https://doi.org/10.5194/acp-11-3137-2011>, 2011.

904 Keller, C. A., Long, M. S., Yantosca, R. M., Da Silva, A. M., Pawson, S., and Jacob, D. J.: HEMCO v1.0: a
905 versatile, ESMF-compliant component for calculating emissions in atmospheric models, *Geosci. Model
906 Dev.*, **7**, 1409–1417, <https://doi.org/10.5194/gmd-7-1409-2014>, 2014.

907 Kirpes, R. M., Bonanno, D., May, N. W., Fraund, M., Barget, A. J., Moffet, R. C., Ault, A. P., and Pratt, K. A.:
908 Wintertime Arctic Sea Spray Aerosol Composition Controlled by Sea-Ice-Lead Microbiology, *ACS Cent.
909 Sci.*, **5**, 1760–1767, <https://doi.org/10.1021/acscentsci.9b00541>, 2019.

910 Leaitch, W. R., Russell, L. M., Liu, J., Kolonjari, F., Toom, D., Huang, L., Sharma, S., Chivulescu, A., Veber,
911 D., and Zhang, W.: Organic functional groups in the submicron aerosol at 82.5° N, 62.5° W from 2012 to
912 2014, *Atmospheric Chem. Phys.*, **18**, 3269–3287, <https://doi.org/10.5194/acp-18-3269-2018>, 2018.

913 Lin, H., Jacob, D. J., Lundgren, E. W., Sulprizio, M. P., Keller, C. A., Fritz, T. M., Eastham, S. D., Emmons, L.
914 K., Campbell, P. C., Baker, B., Saylor, R. D., and Montuoro, R.: Harmonized Emissions Component
915 (HEMCO) 3.0 as a versatile emissions component for atmospheric models: application in the GEOS-
916 Chem, NASA-GEOS, WRF-GC, CESM2, NOAA-GEFS-Aerosol, and NOAA-UFS models, *Geosci. Model Dev.*,
917 **14**, 5487–5506, <https://doi.org/10.5194/gmd-14-5487-2021>, 2021.

918 Liu, H., Jacob, D. J., Bey, I., and Yantosca, R. M.: Constraints from ^{210}Pb and ^7Be on wet deposition and
919 transport in a global three-dimensional chemical tracer model driven by assimilated meteorological
920 fields, *J. Geophys. Res. Atmospheres*, **106**, 12109–12128, <https://doi.org/10.1029/2000JD900839>, 2001.

921 Luo, G. and Yu, F.: Impact of Air Refreshing and Cloud Ice Uptake Limitations on Vertical Profiles and Wet
922 Depositions of Nitrate, Ammonium, and Sulfate, *Geophys. Res. Lett.*, **50**, e2023GL104258,
923 <https://doi.org/10.1029/2023GL104258>, 2023.

924 Luo, G., Yu, F., and Moch, J. M.: Further improvement of wet-process treatments in GEOS-Chem v12.6.0:
925 impact on global distributions of aerosols and aerosol precursors, *Geosci. Model Dev.*, **13**, 2879–2903,
926 <https://doi.org/10.5194/gmd-13-2879-2020>, 2020.

927 May, N. W., Quinn, P. K., McNamara, S. M., and Pratt, K. A.: Multiyear study of the dependence of sea-salt
928 aerosol on wind speed and sea-ice conditions in the coastal Arctic, *J. Geophys. Res. Atmospheres*, **121**,
929 9208–9219, <https://doi.org/10.1002/2016JD025273>, 2016.

930 Monahan, E. C., Spiel, D. E., and Davidson, K. L.: A Model of Marine Aerosol Generation Via Whitecaps
931 and Wave Disruption, in: *Oceanic Whitecaps*, vol. 2, edited by: Monahan, E. C. and Niocaill, G. M.,
932 Springer Netherlands, Dordrecht, 167–174, https://doi.org/10.1007/978-94-009-4668-2_16, 1986.

933 Nilsson, E. D., Rannik, Ü., Swietlicki, E., Leck, C., Aalto, P. P., Zhou, J., and Norman, M.: Turbulent aerosol
934 fluxes over the Arctic Ocean: 2. Wind-driven sources from the sea, *J. Geophys. Res. Atmospheres*, **106**,
935 32139–32154, <https://doi.org/10.1029/2000JD900747>, 2001.

936 Pierce, J. R. and Adams, P. J.: Global evaluation of CCN formation by direct emission of sea salt and
937 growth of ultrafine sea salt, *J. Geophys. Res. Atmospheres*, **111**, 2005JD006186,
938 <https://doi.org/10.1029/2005JD006186>, 2006.

939 Pound, R. J., Sherwen, T., Helmig, D., Carpenter, L. J., and Evans, M. J.: Influences of oceanic ozone
940 deposition on tropospheric photochemistry, *Atmospheric Chem. Phys.*, **20**, 4227–4239,
941 <https://doi.org/10.5194/acp-20-4227-2020>, 2020.

942 Pratt, K. A., Custard, K. D., Shepson, P. B., Douglas, T. A., Pöhler, D., General, S., Zielcke, J., Simpson, W. R.,
943 Platt, U., Tanner, D. J., Gregory Huey, L., Carlsen, M., and Stirm, B. H.: Photochemical production of
944 molecular bromine in Arctic surface snowpacks, *Nat. Geosci.*, **6**, 351–356,
945 <https://doi.org/10.1038/ngeo1779>, 2013.

946 Quinn, P. K., Coffman, D. J., Kapustin, V. N., Bates, T. S., and Covert, D. S.: Aerosol optical properties in the
947 marine boundary layer during the First Aerosol Characterization Experiment (ACE 1) and the underlying
948 chemical and physical aerosol properties, *J. Geophys. Res.*, **103**, 16,547–16,563, 1998.

949 Quinn, P. K., Bates, T. S., Miller, T. L., Coffman, D. J., Johnson, J. E., Harris, J. M., Ogren, J. A., Forbes, G.,
950 Anderson, T. L., Covert, D. S., and Roed, M. J.: Surface submicron aerosol chemical composition: What

951 fraction is not sulfate?, *J. Geophys. Res. Atmospheres*, **105**, 6785–6805,
952 <https://doi.org/10.1029/1999JD901034>, 2000.

953 Quinn, P. K., Miller, T. L., Bates, T. S., Ogren, J. A., Andrews, E., and Shaw, G. E.: A 3-year record of
954 simultaneously measured aerosol chemical and optical properties at Barrow, Alaska, *J. Geophys. Res.*
955 *Atmospheres*, **107**, <https://doi.org/10.1029/2001JD001248>, 2002.

956 Radke, L. F., Hobbs, P. V., and Pinnons, J. E.: Observations of Cloud Condensation Nuclei, Sodium-
957 Containing Particles, Ice Nuclei and the Light Scattering Coefficient Near Barrow, Alaska, *J. Appl. Meteor.*
958 *Climatol.*, **15**, 982–995, [https://doi.org/10.1175/1520-0450\(1976\)015%3C0982:OCCNS%3E2.0.CO;2](https://doi.org/10.1175/1520-0450(1976)015%3C0982:OCCNS%3E2.0.CO;2),
959 1976.

960 Rhodes, R. H., Yang, X., Wolff, E. W., McConnell, J. R., and Frey, M. M.: Sea ice as a source of sea salt
961 aerosol to Greenland ice cores: a model based study, *Atmospheric Chem. Phys.*, **17**, 9417–9433,
962 <https://doi.org/10.5194/acp-17-9417-2017>, 2017.

963 Riley, J. P. and Chester, R.: *Introduction to marine chemistry*, Academic Press, London, New York, 465 pp.,
964 1971.

965 Röhrs, J. and Kaleschke, L.: An algorithm to detect sea ice leads by using AMSR-E passive microwave
966 imagery, *The Cryosphere*, **6**, 343–352, <https://doi.org/10.5194/tc-6-343-2012>, 2012.

967 Roscoe, H. K., Brooks, B., Jackson, A. V., Smith, M. H., Walker, S. J., Obbard, R. W., and Wolff, E. W.: Frost
968 flowers in the laboratory: Growth, characteristics, aerosol, and the underlying sea ice, *J. Geophys. Res.*,
969 **116**, D12301, <https://doi.org/10.1029/2010JD015144>, 2011.

970 Salmi, T.: Measurement of Inorganics in air and particle phase at Pallas (Matorova) (3),
971 <https://doi.org/10.48597/TGMX-CEKH>, 2018.

972 Schmale, J., Zieger, P., and Ekman, A. M. L.: Aerosols in current and future Arctic climate, *Nat. Clim.*
973 *Change*, **11**, 95–105, <https://doi.org/10.1038/s41558-020-00969-5>, 2021.

974 Scott, W. D. and Levin, Z.: Open Channels in Sea-Ice (Leads) as Ion Sources, *Science*, **177**, 425–426,
975 <https://doi.org/10.1126/science.177.4047.425>, 1972.

976 Screen, J. A. and Simmonds, I.: Declining summer snowfall in the Arctic: causes, impacts and feedbacks,
977 *Clim. Dyn.*, **38**, 2243–2256, <https://doi.org/10.1007/s00382-011-1105-2>, 2012.

978 Simpson, W. R., Alvarez-Aviles, L., Douglas, T. A., Sturm, M., and Domine, F.: Halogens in the coastal snow
979 pack near Barrow, Alaska: Evidence for active bromine air-snow chemistry during springtime, *Geophys.*
980 *Res. Lett.*, **32**, 2004GL021748, <https://doi.org/10.1029/2004GL021748>, 2005.

981 Simpson, W. R., Von Glasow, R., Riedel, K., Anderson, P., Ariya, P., Bottenheim, J., Burrows, J., Carpenter,
982 L. J., Frieß, U., Goodsite, M. E., Heard, D., Hutterli, M., Jacobi, H. W., Kaleschke, L., Neff, B., Plane, J., Platt,
983 U., Richter, A., Roscoe, H., Sander, R., Shepson, P., Sodeau, J., Steffen, A., Wagner, T., and Wolff, E.:
984 Halogens and their role in polar boundary layer ozone depletion, *Atmospheric Chem. Phys.*, **7**, 4375–
985 4418, <https://doi.org/10.5194/acp-7-4375-2007>, 2007.

986 Stramler, K., Del-Genio, A. D., and Rossow, W. B.: Synoptically Driven Arctic Winter States, *J. Clim.*, **24**,
987 1747–1762, <https://doi.org/10.1175/2010JCLI2817.1>, 2011.

988 Stutz, J., Thomas, J. L., Hurlock, S. C., Schneider, M., Von Glasow, R., Piot, M., Gorham, K., Burkhart, J. F.,
989 Ziemba, L., Dibb, J. E., and Lefer, B. L.: Longpath DOAS observations of surface BrO at Summit, Greenland,
990 *Atmospheric Chem. Phys.*, **11**, 9899–9910, <https://doi.org/10.5194/acp-11-9899-2011>, 2011.

991 Sumata, H., De Steur, L., Divine, D. V., Granskog, M. A., and Gerland, S.: Regime shift in Arctic Ocean sea
992 ice thickness, *Nature*, **615**, 443–449, <https://doi.org/10.1038/s41586-022-05686-x>, 2023.

993 Swanson, W. F., Holmes, C. D., Simpson, W. R., Confer, K., Marelle, L., Thomas, J. L., Jaeglé, L., Alexander,
994 B., Zhai, S., Chen, Q., Wang, X., and Sherwen, T.: Comparison of model and ground observations finds
995 snowpack and blowing snow aerosols both contribute to Arctic tropospheric reactive bromine,
996 *Atmospheric Chem. Phys.*, **22**, 14467–14488, <https://doi.org/10.5194/acp-22-14467-2022>, 2022.

997 Tan, I., Sotiropoulou, G., Taylor, P. C., Zamora, L., and Wendisch, M.: A Review of the Factors Influencing
998 Arctic Mixed-Phase Clouds: Progress and Outlook, in: *Geophysical Monograph Series*, edited by: Sullivan,
999 S. C. and Hoose, C., Wiley, 103–132, <https://doi.org/10.1002/9781119700357.ch5>, 2023.

1000 Vaughan, D., Comiso, J., Allison, I., Carrasco, J., Kaser, G., Kwok, R., Mote, P., Murray, T., Paul, F., Ren, J. F.,
1001 Rignot, E., Solomina, O., Steffen, K., and Zhang, T.: Observations: Cryosphere, in: *Climate Change 2013:*
1002 *The Physical Science Basis*, 317–382, 2013.

1003 Villanueva, D., Possner, A., Neubauer, D., Gasparini, B., Lohmann, U., and Tesche, M.: Mixed-phase
1004 regime cloud thinning could help restore sea ice, *Environ. Res. Lett.*, **17**, 114057,
1005 <https://doi.org/10.1088/1748-9326/aca16d>, 2022.

1006 Wang, Q., Jacob, D. J., Spackman, J. R., Perring, A. E., Schwarz, J. P., Moteki, N., Marais, E. A., Ge, C.,
1007 Wang, J., and Barrett, S. R. H.: Global budget and radiative forcing of black carbon aerosol: Constraints
1008 from pole to pole (HIPPO) observations across the Pacific, *J. Geophys. Res. Atmospheres*, **119**, 195–206,
1009 <https://doi.org/10.1002/2013JD020824>, 2014.

1010 Wang, X., Jacob, D. J., Downs, W., Zhai, S., Zhu, L., Shah, V., Holmes, C. D., Sherwen, T., Alexander, B.,
1011 Evans, M. J., Eastham, S. D., Neuman, J. A., Veres, P. R., Koenig, T. K., Volkamer, R., Huey, L. G., Bannan, T.,
1012 Percival, C. J., Lee, B. H., and Thornton, J. A.: Global tropospheric halogen (Cl, Br, I) chemistry and its
1013 impact on oxidants, *Atmospheric Chem. Phys.*, **21**, 13973–13996, [https://doi.org/10.5194/acp-21-13973-](https://doi.org/10.5194/acp-21-13973-2021)
1014 2021, 2021.

1015 Wang, Y., Jacob, D. J., and Logan, J. A.: Global simulation of tropospheric O₃–NO_x–hydrocarbon
1016 chemistry: 3. Origin of tropospheric ozone and effects of nonmethane hydrocarbons, *J. Geophys. Res.*
1017 *Atmospheres*, **103**, 10757–10767, <https://doi.org/10.1029/98JD00156>, 1998.

1018 Willis, M. D., Leaitch, W. R., and Abbatt, J. P. D.: Processes Controlling the Composition and Abundance of
1019 Arctic Aerosol, *Rev. Geophys.*, **56**, 621–671, <https://doi.org/10.1029/2018RG000602>, 2018.

1020 World Meteorological Organization (WMO): *WMO/GAW aerosol measurement procedures, guidelines*
1021 *and recommendations*, WMO, Geneva, 2003.

1022 ~~Yang, X., Neděla, V., Runštuk, J., Ondrušková, G., Krausko, J., Vetráková, L., and Heger, D.: Evaporating~~
1023 ~~brine from frost flowers with electron microscopy and implications for atmospheric chemistry and sea-~~
1024 ~~salt aerosol formation, *Atmospheric Chem. Phys.*, 17, 6291–6303, [https://doi.org/10.5194/acp-17-6291-](https://doi.org/10.5194/acp-17-6291-2017)~~
1025 ~~2017, 2017.~~

1026 ~~Zhang, L., Gong, S., Padre, J., and Barrie, L.: A size-segregated particle dry deposition scheme for an~~
1027 ~~atmospheric aerosol module, *Atmos. Environ.*, 35, 549–560, 2001.~~

1028